

**UNMANNED AERIAL VEHICLE REMOTE SENSING TECHNOLOGY FOR
STRUCTURAL DAMAGE ASSESSMENTS IN LOW-LIGHT CONDITIONS**

by

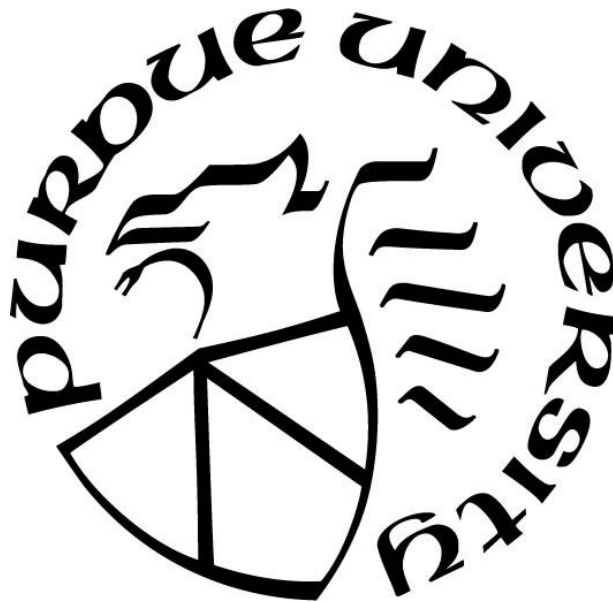
Christopher A. Baker

A Dissertation

Submitted to the Faculty of Purdue University

In Partial Fulfillment of the Requirements for the degree of

Doctor of Philosophy



Department of Technology

West Lafayette, Indiana

August 2019

**THE PURDUE UNIVERSITY GRADUATE SCHOOL
STATEMENT OF COMMITTEE APPROVAL**

Dr. Randy R. Rapp, Chair

School of Construction Management Technology

Dr. Emad Elwakil

School of Construction Management Technology

Dr. Jiansong Zhang

School of Construction Management Technology

Dr. Eric Dietz

School of Computer Information Technology

Approved by:

Dr. Kathy Newton

Head of the Graduate Program

Thank you to my family, without your love and support I would never had made it this far

ACKNOWLEDGMENTS

Thank you to Dr. Robert Cox for the approval to purchase the equipment required for the research to complete my dissertation.

Thank you to Dr. Connor for the use of the S-BRITE center. The facility provided ample specimens for this research.

TABLE OF CONTENTS

LIST OF TABLES	8
LIST OF FIGURES	9
ABSTRACT	11
CHAPTER 1. INTRODUCTION	12
1.1 Scope.....	12
1.2 Significance	13
1.3 Statement of the Problem.....	18
1.4 Research Questions.....	19
1.5 Assumptions.....	19
1.6 Limitations	20
1.7 Delimitations.....	20
1.8 Definitions	21
1.9 Acronyms.....	22
1.10 Summary.....	22
CHAPTER 2. LITERATURE REVIEW	23
2.1 Post-Disaster Reconstruction.....	23
2.2 sUAS Applications in Construction.....	29
2.3 sUAS in Infrastructure	31
2.3.1 Georgia Department of Transportation (2014)	31
2.3.2 Florida Department of Transportation. (2015).....	31
2.3.3 Minnesota Department of Transportation (2015 & 2017)	32
2.3.4 Utah Department of Transportation	33
2.3.5 Michigan Department of Transportation.....	33
2.3.6 Kansas Department of Transportation	33
2.3.7 Oregon Department of Transportation.....	34
2.4 sUAS for Disaster Mitigation	34
2.4 Chapter Summary	41
CHAPTER 3. FRAMEWORK AND METHODOLOGY	43
3.1 Framework	43

3.2 Equipment.....	44
3.2.1 Selection of Small Unmanned Aerial System.....	44
3.2.2 Small Unmanned Aerial System	45
3.2.2.1 Small Unmanned Aerial Vehicle	46
3.2.2.2 Small Unmanned Aerial Vehicle Optics.....	47
3.2.2.3 Small Unmanned Aerial Vehicle Ground Control Station	48
3.2.2.4 Flight Mode for Experiments.....	49
3.3 Experiment Methodology	49
3.3.1 Procedure for sUAS Steel Bridge Component Experiment	49
3.3.2 Selection of Steel Bridge Components	49
3.3.3 Experimental Process.....	50
3.3.3.1 Initial Flight Test.....	51
3.3.3.2 Preliminary Field Experiment.....	52
3.3.3.3 Low-Light Inspection Distance Experiment.....	53
3.3.3.4 Validation Distance Experiment	56
3.4 Unit of Analysis	57
3.5 Data Collection	57
3.6 Threats to Validity	57
3.7 Data Analysis	58
3.8 Chapter Summary	58
CHAPTER 4. DATA ANALYSIS AND RESULTS	60
4.1 Initial Flight Test	60
4.2 Visual Data of sUAS Imagery	61
4.2.1 Preliminary Field Test of Steel Bridge Members at S-BRITE	61
4.2.1.1 Preliminary Field Test - Norfolk Southern Railroad (NSR) Deck Girder Span ...	64
4.2.1.2 Preliminary Field Test – Virginia Avenue Bridge.....	67
4.2.2 Low-Light Inspection Distance.....	71
4.2.2.1 Low-light Inspection Distance Imagery.....	73
4.2.2.3 Low-light Inspection Distance Tabular Data	80
4.2.3 Validation Test.....	85
4.3 Analysis	90

4.3.1 Research Question One Data	90
4.3.2 Research Question Two Data.....	91
4.3.3 Research Question Three Data.....	95
4.4 Summary	96
CHAPTER 5. DISCUSSION.....	97
5.1 Major Findings.....	97
5.1.1 Preliminary Field Test.....	97
5.1.2 Low-Light Inspection Distance Findings.....	98
5.1.3 Validation Findings.....	99
5.2 Discussion.....	100
5.2.1 Preliminary Field Test.....	100
5.2.2 Low-Light Inspection Distance.....	101
5.2.3 Validate Experiment	102
5.3 Conclusion	102
5.4 Recommendations.....	105
5.5 Summary.....	108
REFERENCES	14
PUBLICATION.....	20

LIST OF TABLES

Table 1: Yuneec H520 UAV specifications.....	47
Table 2: CGOET camera specifications	47
Table 3: ST16S ground control station.	48
Table 4: Defects recorded for each time interval at known distance	83
Table 5: Defects observed during nautical twilight at known distances.....	83
Table 6: Defects observed during astronomical twilight at known distances.....	84
Table 7: Defects observed during night at known distances.....	84
Table 8: Validation data of defect observed at seven feet (2.13m)	89
Table 9: Analysis of variance of defect versus time.	91
Table 10: Defects versus time model summary.....	91
Table 11: Analysis of variance defects versus distance.....	93
Table 12: Model Summary of defects versus distance.	93
Table 13: Analysis of variance of defects versus time and distance.....	94
Table 14: Model Summary of Defects versus time and distance.....	94
Table 15: Coefficients of Defects versus time and distance.	94
Table 16: Pearson Correlation for defects, time, and distance.	96

LIST OF FIGURES

Figure 1: Number of steel versus total bridge failed due to external causes 2000-2012.....	14
Figure 2: Yuneec H520 UAV, CGOET camera, and ST16S ground control station.	46
Figure 3: sUAS flight controls flow chart prior to each experiment.	52
Figure 4: Low-light distance experiment diagram.....	55
Figure 5: Steel Girder experiments flow chart.....	55
Figure 6: Validation experiment diagram.	56
Figure 7: Bowen Laboratory initial flight test.	61
Figure 8: Steel bridge members at S-BRITE: (a) Norfolk Southern Railroad deck plate girder span; (b) Virginia Avenue bridge girder.	62
Figure 9: RGB low-light camera image of 0.748 inch (19 mm) hole in web steel girder span D234.	65
Figure 10: Thermal image of 0.748 inch (19 mm) in web of NSR steel girder span D234 (rainbow pallet).	66
Figure 11: Thermal image of 0.748 inch hole in web of NSR steel girder span D234 (white hot pallet).	67
Figure 12: RGB low-light image of crack in web of Virginia Avenue bridge steel girder.	69
Figure 13: Thermal image of crack in web of Virginia Avenue steel girder (rainbow pallet).	70
Figure 14: Thermal image of crack in web of Virginia Avenue steel girder (white hot pallet) ...	71
Figure 15: Thermal camera images of Virginia Ave girder from 6 ft: (a) Nautical twilight; (b) Astronomical Twilight; (c) Night.	73
Figure 16: Low-Light RGB camera images of Virginia Ave girder from 4 ft: (a) Nautical twilight; (b) Astronomical Twilight; (c) Night.....	74
Figure 17: Low-Light RGB camera images of Virginia Ave girder from 6 ft: (a) Nautical twilight; (b) Astronomical Twilight; (c) Night.....	75
Figure 18: Low-Light RGB camera images of Virginia Ave girder from 8 ft: (a) Nautical twilight; (b) Astronomical Twilight; (c) Night.....	75

Figure 19: Low-Light RGB camera images of Virginia Ave girder from 10 ft: (a) Nautical twilight; (b) Astronomical Twilight; (c) Night.....	76
Figure 20: Low-Light RGB camera images of Virginia Ave girder from 12 ft: (a) Nautical twilight; (b) Astronomical Twilight; (c) Night.....	76
Figure 21: Low-Light RGB camera images of Virginia Ave girder from 14 ft: (a) Nautical twilight; (b) Astronomical Twilight; (c) Night.....	77
Figure 22: Low-Light RGB camera images of Virginia Ave girder from 16 ft: (a) Nautical twilight; (b) Astronomical Twilight; (c) Night.....	78
Figure 23: Low-Light RGB camera images of Virginia Ave girder from 18 ft: (a) Nautical twilight; (b) Astronomical Twilight; (c) Night.....	79
Figure 24: Low-Light RGB camera images of Virginia Ave girder from 20 ft: (a) Nautical twilight; (b) Astronomical Twilight; (c) Night.....	79
Figure 25: Damage and defects in Virginia Ave steel girder.....	81
Figure 26: Defects versus time and distance.....	81
Figure 27: Low-Light RGB (a) and thermal (b) camera images of southwest side of the Virginia Ave girder during nautical twilight from 8 ft.....	86
Figure 28: Low-Light RGB (a) and thermal (b) camera images of northwest side of Virginia Ave girder during nautical twilight from 8 ft	86
Figure 29: Low-Light RGB (a) and thermal (b) camera images of southwest side of Virginia Ave girder during astronomical twilight from 8 ft (2.44m).	87
Figure 30: Low-Light RGB (a) and thermal (b) camera images of northwest side of Virginia Ave girder during astronomical twilight from 8 ft (2.44m).	87
Figure 31: Low-Light RGB (a) and thermal (b) camera images of southwest side of Virginia Ave girder during night from 8 ft (2.44m).	88
Figure 32: Low-Light RGB (a) and thermal (b) camera images of northwest side of Virginia Ave girder during night from 8 ft (2.44m).	89
Figure 33: Regression equation for defects versus distance.	93
Figure 34: Regression equation for defects versus time and distance.	95

ABSTRACT

Author: Baker, Christopher, A. PhD

Institution: Purdue University

Degree Received: August 2019

Title: Unmanned Aerial Vehicle Remote Sensing Technology for Structural Damage Assessments in Low-Light Conditions.

Major Professor: Dr. Randy R. Rapp

The research explores the viability of using a small Unmanned Aerial Vehicle equipped with thermal imaging and lowlight camera to assess structural damage to steel girders. Damage assessments following natural disasters are daunting and arduous tasks that are resources intensive and dangerous. Unmanned aerial vehicles with remote sensing technology (UAV-RS) have been used in recent large-scale disaster events such as Hurricanes Katerina, Harvey, Irma, and Maria as well as others. Current assessment methods of structures include; inspectors physically conducting detailed and rapid surveys of damage with or without the assistance of special equipment, use of helicopters, satellite imagery, and new innovative methods using unmanned aerial vehicles with remote sensing technology.

The initial experiment utilized the S-BRITE facility at Purdue University. Two steel girders located at S-BRITE were used in the experiment with damages that render them structurally deficient. Experiments were conducted during hours of low visibility.

Most scientific studies have focused on using UAV-RS during hours of daylight. This research explores the use of UAV-RS during low-light conditions (i.e. early evening nautical and astronomical twilight, and night) for detecting global damage to steel girders. The goal is to present evidence for further study in the use of UAV-RS during low-light conditions for inspecting structures to include primary load bearing members. The research concluded that while the UAV-RS can detect global damage in low visibility conditions, further experiments in varying low-light conditions to include 3D imaging and semi-autonomous inspection using computer vision are important for structural damage assessments.

CHAPTER 1. INTRODUCTION

This chapter provides an overview of the research and the dissertation. The purpose was to establish the scope, significance, and statement of the problem for research using small unmanned aerial system to assess damage and defects in low-light conditions. Key terms and acronyms are defined as well as assumptions, limitations, and delimitations.

1.1 Scope

The scope of research establishes the capability of utilizing small unmanned aerial systems equipped with remote sensing technologies (sUAS). Remote sensing technologies provide the ability to obtain situational awareness following a disaster event without be physically present at the location be investigated. The purpose of utilizing sUAS was to gain situational awareness of damage to road infrastructure in areas inaccessible to personnel during low-light conditions. sUAS have the potential to assist in recovery efforts and better assess, plan, prepare, and execute recovery activities immediately following a disaster. The ability to gain better situational awareness using sUAS can ultimately improve recovery efforts through qualifying damage to bridges which are critical ground transportation routes. The paper used a quantitative methods research design to investigate the use of sUAS in low-light conditions.

First, the study explored the use of sUAS, and remote sensing technologies currently used in the construction, infrastructure assessment and disaster response. A literature review of the current methods of using sUAS and remote sensing technologies in construction projects and, the accuracy of the information remote sensing provides.

Based on the literature review of sUAS use in construction, infrastructure, and disaster recovery, the research proposed utilizing sUAS with remote sensing technology to assess damage and defects in steel bridge girders in low-light conditions.

Second, the study used data derived from experiments using sUAS with RGB low-light and thermal imaging camera to conduct assessments of damage and defects in steel girders during low-light conditions. The imagery of the RGB low-light and thermal imaging camera was compared with one another and assessed against the known damage and defects.

Third, the study used data derived from the prior experiment using the sUAS with RGB low-light and thermal imaging camera, conducting an experiment on the effect of distance during low-light conditions observing damage and defects in steel bridge girders. An experiment based on traditional methods using known distances was used to obtain the effects. This base of knowledge was used to determine if the sUAS with RGB low-light and thermal imaging camera was capable of observing damage and defects in steel bridge components.

1.2 Significance

The findings of this research redounded to the aid of bridge inspection post disaster, as sUAS equipped with remote sensing technologies play an important role in post disaster assessments. The greater demand for situational awareness following a disaster necessitates leveraging technologies to ascertain the status of road infrastructure, as these serve as important arteries for response and recovery operations.

Over the last decade, extreme weather events have had an increasing economic effect on the United States, costing approximately \$724.4 billion in damages (NOAA,

2018). Of these extreme weather events, flooding, freeze, severe storms, and winter storms have accounted for \$198.8 billion in damages. Following these extreme weather events, the reduced capacity of road infrastructure affects response and recovery efforts.

Bridges are a critical component of road infrastructure, connecting. A study of bridge failures between 1980 and 2012 in the United States found 94 percent of the 1,062 bridge failures occurred during service and 59 percent were partial or complete failures. The top five external cause for bridge failures between 1980 and 2012 were: 1) Flood; 2) Scour; 3) Collision; 4) Overload 5) Environmental degradation (Lee *et al.*, 2013). All five of these conditions are exacerbated during disaster events involving extreme weather. Bridges are a critical component of road infrastructure and therefor the ability to assess their damage following a disaster is essential for response and recovery operations.

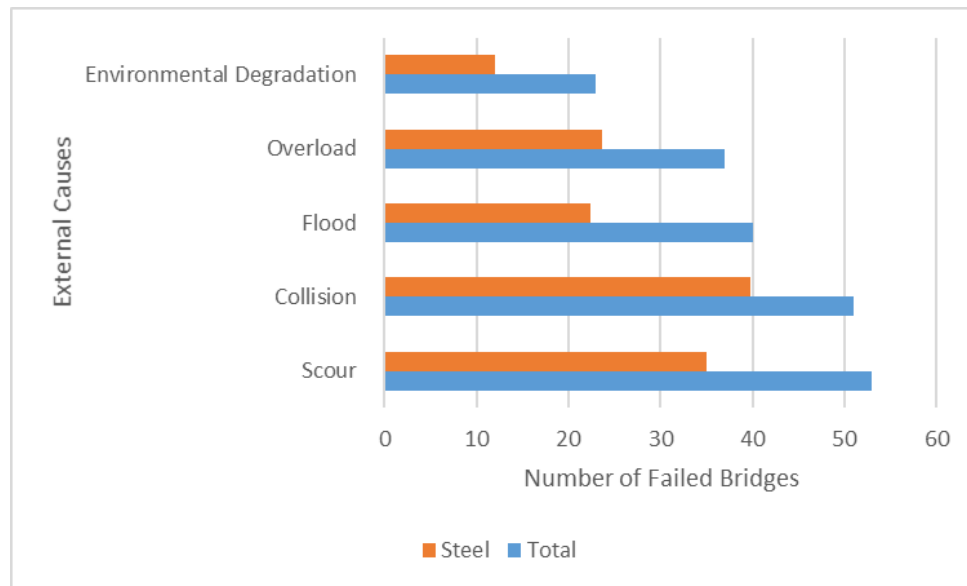


Figure 1: Number of steel verse total bridge failed due to external causes 2000-2012.

Damage inspections are required after disaster events – whether environmental or manmade – to assess the structural integrity of the bridge. Damage inspection reports

require enough information to determine whether to implement emergency load restrictions or closure of the bridge and the level of effort required to repair the bridge (BIRM, 2012). Conducting bridge damage inspections following a disaster event can be an arduous task as the affected could include several hundred bridges located in areas of high population density. These bridges often control access to emergency services and health care facilities, in addition to power stations and sub stations, gas refineries, and chemical plants.

Following a disaster event such as a hurricane or major earthquake, the traditional inspection methods for inspecting bridge superstructures – aerial work platforms, use of ladders, scaffolding, rigging, and catwalks and travelers – require inspectors to have accessibility to bridges and thus rely on alternate means such as satellite or aerial (helicopter) imagery to conduct initial damage inspections.

Sensing technology such as ground penetrating radar (GPR), light detection and ranging (LiDAR), and unmanned aerial vehicles with remote sensors (UAV-RS) have been developed and studied to assist in inspecting bridges. Of these sensing technologies, UAV-RS has a remote capability to inspect bridges that are not immediately accessible.

Between 2005 and 2014 the United States experienced 212 disasters – second only to China, with a price tag of \$443 billion – first in economic loss. Worldwide 1.7 million people were affected by natural disasters and damages totaling \$1.4 trillion due to natural disasters (UNISDR, 2017). The increase in economic and human cost of disasters has led nations to improve response and recovery measures to mitigate losses and speed recovery.

Furthermore, this research would benefit first responders in assessing viable routes for egress and rescue operations. Hurricane Katrina is one of the deadliest and costliest storms to ever strike the United States. Deaths attributed to hurricane Katrina were estimated to be 2,000 throughout the affected area. The death toll ranked Katrina as the third deadliest in United States history behind the 1900 Galveston hurricane and the 1928 Lake Okeechobee hurricane. This research seeks to minimize loss of life following a disaster event utilizing UAV-RS and a model developed to assist in predicting the best route based off information provided by UAV-RS. Hurricane Katrina displaced more than a million people from the affected area, of people initially displaced 600,000 were still displaced a month later. New Orleans lost over half of its population following the hurricane and by 2015 roughly 20 percent had yet to return. Contributing to the decline was the millions of homes damaged by Katrina. Estimates of 70 percent of all occupied units in the city of New Orleans were damaged.

The National Preparedness Goal of a secure and resilient nation with the capabilities required across the whole community to prevent, protect against, mitigate, respond to, and recover from the threats and hazards that pose the greatest risk, defines what is meant by the whole community to be prepared (DHS, 2013). Successful recovery from disasters is measured in terms of lives saved, mitigation of further damage to property and the environment, meeting basic human needs, stabilizing the incident, the restoration of basic services and community functionality, and establishing a safe and secure environment to facilitate reconstruction and restoration.

The compilation of known knowns (things we know), unknown knowns (things we know we don't know), and unknown unknowns (things we do not yet know we don't

know) makes planning, preparing, and recovering from disasters a complex and dynamic undertaking. The primary function of emergency management professionals is to prepare for disaster (McEntire, Boudrot, & Webb, 2015). Preparing for a disaster requires knowledge of types of disasters possible and the probability of occurrences. Although professionals supply tacit and expert knowledge in disaster planning and recovery from past events, ensuring appropriate methodologies are used during response operations, it is impossible to predict the extent of damage from a disaster and the areas affected the most.

Accurate and timely information following a disaster event is a critical part of the recovery and requires detailed information to make accurate and timely decisions for the restoration of essential services and infrastructure. Hazardous conditions resulting from geophysical (e.g., earthquake and volcanos), hydrological (e.g., flood and storm surge), meteorological (e.g., hurricanes and tornadoes), climatological (e.g., wildfire and glacial lake burst), or biological (e.g., epidemic and bio-agents) delay information of damage assessments due to a lack of accessibility to affected areas.

Damage assessments during disaster recovery is a critical information requirement of recovery operations. Detailed disaster damage assessments enable resources to be allocated in an effective manner by supplying the information necessary to address the direst situations first. The adoption of unmanned aerial vehicles (UAV) using 3-dimensional mapping for surveying damage following a disaster event has proven an effective tool. This research expanded upon past work with UAV 3-dimensional mapping by experimenting with a dual sensor thermal imaging and RGB low-light camera in low-light conditions.

1.3 Statement of the Problem

With approximately 40 percent of bridge in the United States over 50 years old, the type of bridges failing, and the cause of failure is important to understand. According to a study on bridge failures in the United States from 1980 thru 2012, 94 percent of the 1,062 bridge failures occurred during service and 59 percent of the bridge failures were partial or complete failures (Lee, *et al.*, 2013). The high percentage of bridges failing during service, demonstrates the need for improved inspection methods.

The risk of bridges failing during service increases following a disaster event. Damage sustained to a bridge primary load bearing member reduces the load capacity of the bridge, increase the occurrence of a partial or complete collapse from vehicle traffic attempting to evacuate or emergency vehicles responding. Erdelj *et al.* affirmed the use of UAVs following a disaster event to enable practitioners to assess structures for damage and assist in determining the extent of damage (2017). Emergency response and evacuations occur all hours of the day during disasters, so the ability to assess bridge damage during low-light conditions is necessary. Several experts agree that emergency operational plans are a crucial component of emergency management (Lee, Woests, & Heath, 2007). The literature shows extensive research in the use of sUAS for bridge inspections, disaster response and recovery. However, there is a lack of research in the use of UAV-RS inspection of bridges during low visibility conditions. Vaghefi *et al.* (2012) noted their literature review found no studies of surface defects using thermal imaging.

Adapting an innovative solution, using sUAS in low-light conditions, enables recovery operations to continue around the clock. To future researchers, this research can

provide a baseline of information to expand upon using sUAS in low-light conditions to assess damage and defects in low-light conditions.

1.4 Research Questions

1. What is the effect of low-light conditions on the sUAS optics to assess global structural damage?
2. What effect does distance have on the sUAS camera imagery in observing damage and defects in the structural steel during low-light conditions?
3. What is the logical correlation, if any, between the sUAS camera imagery to observe damage and defects during low-light conditions at a given distance?

1.5 Assumptions

The research and findings are derived subscribing to the following assumptions:

1. Current sUAS methods for post-disaster bridge assessments do not use RGB low-light and thermal imaging technology during low-light conditions.
2. The specific UAV, photogrammetry, and thermal imaging equipment used to obtain post-disaster debris estimates and assessment of bridge conditions will not alter the generalization of the results unless specified.
3. The steel bridge girder samples in the context of the research consist of typical damage that may occur during a disaster event.
4. The UAV, photogrammetry, and thermal imaging equipment was working correctly according to manufactures specifications.

1.6 Limitations

The research was limited by the following:

1. The data obtained from this study is limited to the steel bridge components available at S-BRITE.
2. The study is limited to the quantification of damage and defects based on imagery obtained from the sUAS in a controlled environment.
3. All possible steel bridge component damage and defects are not examined in the research.
4. Parsimony prevents comparisons of multiple sUAS and RGB low-light and thermal imaging technology.
5. The study uses current open source navigation aids for flight planning.

1.7 Delimitations

Research conducted in this study acknowledges the following delimitation:

1. The research is limited to damage and defects samples of steel bridge girders at the S-BRITE facility using the National Bridge Inspection Standards.
2. The steel bridge girders in this research are in a control field environment.
3. A specific sUAS, RGB low-light and thermal imaging camera, and ground control station are used in this research.
4. The research is limited to the examination of damage and defects in steel bridge girders using sUAS during low-light conditions and does not explore GPS denied areas underneath bridges. Further examination of sUAS capabilities in low-visibility conditions would be useful in post-disaster reconstruction and restoration.

1.8 Definitions

Autonomous aircraft - An unmanned aircraft that does not allow pilot intervention in the management of the flight (ICAO, 2011).

Autonomous operation - An operation during which a remotely piloted aircraft is operating without pilot intervention in the management of the flight (ICAO, 2011).

Command and control link - The data link between the remotely piloted aircraft and the remote pilot station for the purposes of managing the flight (ICAO, 2011).

Lost link - The loss of command and control link contact with the remotely piloted aircraft such that the remote pilot can no longer manage the aircraft's flight (ICAO, 2011).

Mitigation - reduce the loss of life and property by lessening the impact of future disasters (NRF, 2013).

National Response Framework - a guide to how the Nation responds to all types of disasters and emergencies (NRF, 2013).

National Incident Management System - systematic, proactive approach to guide departments and agencies at all levels of government, nongovernmental organizations, and the private sector to work together seamlessly and manage incidents involving all threats and hazards (NRF, 2013).

Operational control - The exercise of authority over the initiation, continuation, diversion or termination of a flight in the interest of safety of the aircraft and the regularity and efficiency of the flight (ICAO, 2011).

Prevention - avoid or stop an imminent, threatened or actual act of terrorism (NRF, 2013).

Protection - citizens, residents, visitors and assets against the greatest threats and hazards in a manner that allows United States interests, aspirations and way of life to thrive (NRF, 2013).

Radio line-of-sight - A direct electronic point-to-point contact between a transmitter and a receiver (ICAO, 2011).

Recovery - the timely restoration, strengthening and revitalization of infrastructure, housing and a sustainable economy, as well as the health, social, cultural, historic and environmental fabric of communities affected by a catastrophic incident (NRF, 2013).

Remotely piloted aircraft - An aircraft where the flying pilot is not on board the aircraft (ICAO, 2011).

Response - save lives, protect property and the environment, and meet basic human needs in the aftermath of a catastrophic incident (NRF, 2013).

Segregated airspace - Airspace of specified dimensions allocated for exclusive use to a specific user(s) (ICAO, 2011).

Unmanned aircraft - An aircraft which is intended to operate with no pilot on board (ICAO, 2011).

Unmanned aircraft system - An aircraft and its associated elements which are operated with no pilot on board (ICAO, 2011).

Visual line-of-sight operation - An operation in which the remote crew maintains direct visual contact with the aircraft to manage its flight and meet separation and collision avoidance responsibilities (ICAO, 2011).

1.9 Acronyms

GPS – Global Positioning Satellites

sUAS – Small Unmanned Aerial Vehicles

RGB – Red, Blue, and Green

UAV-RS – Unmanned Aerial Vehicle with remote sensing

1.10 Summary

The research paper explored the possibilities of improving damage assessment along routes by using UAV-RS technologies to quantify and qualify damage and defects to bridge steel members for proper resource allocation and route trafficability by testing UAV-RS on steel bridge samples. The following chapter conducts a literature review of UAV-RS in construction, infrastructure inspections, and disaster operations.

CHAPTER 2. LITERATURE REVIEW

Following a systematic review of literature, the scope of the literature review was limited to post-disaster recovery operations in reconstruction, UAV-RS use in the construction industry, and the use of UAV-RS following a disaster event. Research studies that did not fit the focus of this research were not included in the literature review. The review of literature was an attempt to find research covering surveying road infrastructure and any gaps in the body of knowledge.

2.1 Post-Disaster Reconstruction

Traditional construction projects require a unique set of skills and attributes focus of solving problems throughout the project as they develop. Projects are a unique conglomeration of constraints defined by specifics such as duration, quality, budget, construction team, location, and others. Each project, no matter the size, offers a unique set of challenges to include site conditions, weather, subcontractors, and labor issues on site. In the end a project is measured by four metrics; time, cost, quality, and safety but communication, relationships, coordination and collaboration are essential during the project (Boyd & Chinyio, 2008). Construction is resource intensive consuming manpower, machines, material, and money, requiring timely and efficient management of these finite resources. To manage these resources requires project controls focused on time, costs, quality, and safety. Project planning enables effective project controls by defining scope and tasks, assigning responsibility, and allocating resources. Through project planning, management can track and control time and costs.

Between 2005 and 2014 the United States experienced 212 disasters – second only to China and a price tag of \$443 billion, ranking first in economic loss. There were 1.7 billion people worldwide affected by natural disasters between 2005 and 2014. Worldwide damages from disasters totaled \$1.4 trillion (UNISDR, 2017). Over the last decade several advances in disaster preparedness and response have come about, building a library of knowledge based on lessons learned (Lloyd-Jones, 2006). Disaster mitigation measures - early warning, planning, and preparing - has improved over the last 12 years. Disaster response is essential in mitigating loss of life and damage to property and infrastructure. Initial damage estimates from a disaster is often based upon historical data from past disaster events of similar type combined with assessments conduct on-site and a common factor in all disasters is the rapid removal of debris (Rapp, 2008). Professional emergency management practitioners apply tacit knowledge in planning and preparing for disasters, ensuring the appropriate response level in the event of a disaster. Furthermore, government agencies and non-governmental agencies are attempting to close the gap between relief and long-term recovery efforts of reconstruction and development (Lloyd-Jones, 2006). Damage estimates among all the effected countries of the Indian Ocean tsunami of 2004 was between \$10 to \$11 billion of which 80 percent is attributed to reconstruction and long-term recovery (TRN, 2005, Annex 4, p.35).

Recovery as defined by the Federal Emergency Management Agency is “those capabilities necessary to assist communities affected by an incident to recover effectively” (DHS, 2016, p. 1). Planning and plans are indispensable to post-disaster restoration and reconstruction. Because planners are not clairvoyant, plans for disaster recovery are preliminary estimates based on available data with contingencies built in for

additional unknowns. Preliminary estimates of damage from post-disaster information Smith (2010) asserts, is often incomplete, based on a snapshot in time, subject to change at moment's notice. The incompleteness of estimates has a cascading effect regarding resources, consequently delaying the post-disaster restoration and reconstruction effort.

Post-disaster recovery presents stakeholders with dynamic and complex problems. With uncertainty as a pervasive factor in post- disaster recovery; analysis of debris and damage is limited to visual inspection on the ground or through the use of aircraft or video/images provided by UAVs. While personnel inspection via manned aircraft and UAV video provide a degree of clarity, they lack the ability to accurately quantify debris or assess damage of critical highway infrastructure - further complicating the recovery process. Analyzing post-disaster recovery through the allocation of resources (manpower, equipment, materials, and costs) is necessary to understand issues hindering the recovery process. Research identified market-related constraints on resources in post-disaster reconstruction such as, competition among aid agencies, local availability and capacity, coupled with economic factors affecting supply and demand making some materials cost prohibitive (Chang, Wilkinson, Regan, & Seville, 2012). Current production rates are based off current global demand and future demand making black swan events like disaster reconstruction subject to current market conditions. The need to rapidly assess the post-disaster environment is essential providing suppliers the information necessary to increase production.

Updates in building codes has impacted the demand on resource availability and is compounded exponentially following a disaster event. Several researchers found policy makers often overlook the impacts of legislation updating building codes on disaster

reconstruction and they tertiary impact to existing manufacturing systems, current construction industry practices, and the built environment (Burby, 2006; Chang-Richards *et al.*, 2012; Haig *et al.*, 2006; Rotimi *et al.*, 2009; Spence, 2004). In historic districts and urban blight areas the impacts of code changes on the cost to rebuild becomes apparent when restoration and reconstruction begins.

Gaining situational awareness or “ground truth”, is vital in assessing any phase of disaster recovery. In post-disaster restoration and reconstruction “ground truth” affords stakeholders the knowledge to plan – creating a “common operating picture” of debris needing to be removed and damage infrastructure needing repaired and/or reconstruction. Current methods for obtaining the “ground truth” following a disaster is derived from incident command, a central location where organizations made up of first responders, local, state, and federal agencies, media, NGOs, and the local community place liaisons to develop a common operating picture. While the information gathered at the incident command post provides assessments and clarity to understanding the totality of the affected area the information developed is incomplete to maximize resource allocation. The lack of detail in the information distorts the “common operating picture” leaving organizations beholden to hierarchal means of control, creating an unbalanced information process devoid of the level of operational feedback necessary to correct errors (Comfort, 2007).

Incomplete information regarding damage assessments and debris estimation hinder recovery planning and operations. Research indicates when contractors do not have a clear picture on the scope of work, time and costs climb rapidly (Rapp, 2008). Research has shown government to be a key facilitator in post-disaster recovery with

respect to resource availability and management (Chang, Wilkinson, Potangaroa, & Seville, 2012). Incomplete information requires assumptions to supplement decisions and may lead to the misallocation of resource. Asynchronous dissemination of vital information causes multiple organizations involved in disaster response and recovery operations to respond without situational awareness (Comfort, 2007). Responding without situational awareness further delays allocation and reacquisition of additional resources needed for recover, repair, and reconstruction. Smith (2010) highlights, local and state governments lack of capability to provide reliable estimates required to obtain the necessary resources from the federal government, non-government organizations, foundations, corporations, and insurance companies hinders response and recovery following a disaster.

A study by Baroudi and Rapp (2014) showed 81 percent of restoration contractors cited insurance adjuster approvals pertain to project scope and cost as a main reason for delays. Delays in approving projects leads to delays in procurement of the resources (e.g., material, labor, and equipment). Large-scale disasters spike the demand for construction resources (Chang *et al.*, 2012) going beyond the regions existing supply capacity (Koria, 2009) due in part to urgency to return displaced persons to their homes, further stressing the demand on building materials (Decon, 2007 & Boen, 2008). The compounding effects of incomplete information, unreliable estimates, lack of timely funding, and scarcity of resources exponentially increase the time to recover after a disaster event.

Researchers found post-disaster transportation systems were vital to obtaining the required resources for recovery operations (Chang *et al.*, 2012). Infrastructure, a critical component in disaster recovery operations, requires a rapid and accurate assessment to

establish a means for personal to deliver supplies and begin restoration or reconstruction. Rapid assessment of critical highway and road infrastructure such as bridges provide information to make decisions to whether routes are impassable and alternative measures such as, float bridges or airlifts are required to facilitate delivery of supplies. Following the 2005 tsunami in Indonesia a key road in Banda Aceh connecting to the housing area was impassible (Chang *et al.*, 2012), with the capability to rapidly assess the situation alternate measures could be have implemented sooner, potentially saving lives.

Traditional methods used by government agencies for estimating damage and debris are based off formulas and rules-of-thumb (Rapp, 2011). These estimates require personnel have access to the area requiring estimation. Post-disaster areas were debris, flood waters, fire, chemical, biological, radiological, nuclear, and explosive hazards are present – prohibit personnel from conducting surveys on-site. In scenarios like these where access via land is not a viable option, government agencies often deploy manned aircraft to conduct response and recovery efforts which is highly expensive (Reich, 2016). Furthermore, past research in disaster recovery and reconstruction has identified the need to further study factors interrupting resource availability and seek solutions to increase resource procurement lead times and production capacity (Chang *et al.*, 2012).

Researchers have recognized the need for better collaboration and coordination between government and the construction industry in address resources shortages resulting from disasters (Chang *et al.*, 2012; Comerio, 2004; Zhang & Peacock, 2010). Therefore, the use of UAVs has gained increasing interest from disaster practitioner and researchers. The role of UAV-RS has increased rapidly over the last five years regarding applications in assessing and estimating in construction as well as disaster events.

2.2 sUAS Applications in Construction

Knowledge and accuracy of costs are imperative in construction to predict profitability of a given project. Drones (UAV) provide construction firms the ability to save costs through reduced man-hours, improved estimates, and reduced risk. UAVs provide real time information to contractor of the ground truth. UAVs equipped with remote sensing technology (UAV-RS) can provide better situational awareness on construction sites. Remote sensing is the use of technology to acquire information about objects or areas from a distance (NOAA 2017). Komatsu, a Tokyo based companies, is using UAV-RS in concert with unmanned bulldozers and excavators – UAV-RS provide detailed volumetric earth estimates for removal (Jensen, 2015). UAVs utilized in the construction industry are classified in mini Unmanned Aerial Systems (UAS) with an operation range of less than 10 kilometers, fly below national ceilings of segregated airspace, with two hours or less of flight time, and less than 30 kilograms of maximum take-off weight (Molina, 2014).

UAV-RS afford construction safety managers the ability to monitor and inspect large constructions sites. UAV-RS carrying high resolution cameras provide real-time images of unsafe acts or conditions on construction projects (Santos de Melo *et al.*, 2017). Safety mangers complete safety inspections in a matter of hours on a large construction project, translating to be able to conduct multiple inspections in a day. Secondary benefit of imagery captured by UAVs is the ability to provide instant feedback on unsafe acts to foreman and supervisors. A tertiary benefit is conducting after action reviews with construction crews, creating teachable movements for lesson learned and reinforcing best practices. UAVs using high resolution cameras for safety inspections on

construction sites as well as inspecting critical infrastructure such as bridges. Li, Zhao, and Ding (2005) found using traditional methods used in bridge inspections were time consuming, expensive, and a high safety risk for the personnel, where UAVs were fast, inexpensive, and eliminated personnel risk.

Santos de Melo *et al.* (2017) used a UAV on a residential low-income housing project in Brazil. The site was 150,000 square meters with 91 five story buildings and five three story building with 600 construction workers. In a little over two hours they collected 579 pictures, of which 53 were used for safety inspection. Examples of safety violations captured were: waste unprotected from rain, workers without hard hats and personnel fall arrest systems, safety platforms not installed on the entire perimeter of buildings, workers on roofs not tied off, workers not wearing hard hats, and lack of traffic control in material handling areas (Santos del Melo *et al.*, 2017).

UAVs equipped with high resolution cameras coupled with point cloud software have successfully conducted field surveys. Using UAVs to take volumetric estimates reduces costs by providing a quick and accurate survey – 10 minutes per 100 acres - compared to less accurate estimates based of previous work or truck counts (Zhang, 2017). Research indicates when contractors do not have a clear picture on the scope of work, time and cost climb rapidly (Rapp, 2008). UAV-RS provides the capability to estimate debris immediately with 3-D mapping technology. Seibert and Teizer (2014) found mobile 3-D mapping for surveying earthwork took one third of the time of traditional survey methods and covered an additional 10,570 square meters. A critical component of accurate 3-D mapping is in the mission planning. Due to the sensitivity to wind and wind burst, micro- and mini-UAVs mission plans require large forward (80%)

and cross (60 - 80%) overlap to adjust lack of stability (Molina, 2014). Seibert and Teizer (2014) successful estimated quantities of dirt in earth moving operations using a UAV equipped with a high-resolution camera, photogrammetry software, and flight path planning software flying semi-autonomously. Omar and Nehdi (2017) found using infrared cameras on a UAV are capable of detecting defects in concrete deck bridges.

2.3 sUAS in Infrastructure

2.3.1 Georgia Department of Transportation (2014)

Irizarry and Johnson (2014) conducted semi-structured interviews with GDOT divisions to establish the requirements for potential uses and types of UAVs required, in addition to a cost benefit analysis. The research team opted for user centric approach to establish the potential uses of UAVs by each division. The application of UAVs primarily focused on the use in traffic monitoring and surveillance. The results from the interviews was used in conjunction with different UAS designs and characteristics to establish five potential UAS for the requirements of each GDOT division.

2.3.2 Florida Department of Transportation. (2015)

Otero *et al.* study the use of drones for inspecting bridges and high mast poles. The study sought to establish sUAS limitations in controlled wind environments, image quality in different flight scenarios and low-light conditions for use in structural inspections. The flight characteristics of the sUAS were study as well, test the effects of attitude on pilot control, payload on flight times based on battery type, and maneuverability test to establish safe operating distances.

2.3.3 Minnesota Department of Transportation (2015 & 2017)

Lovelace (2015) conducted phase one of a two phase demonstration project to evaluate different UAS technologies and its capability to be a safe and effective tool for inspecting bridges. During phase one, they performed test inspection on four bridges of varying sizes and types in Minnesota. Prior to inspections detailed plans were developed for each bridge inspection using a variety of imaging devices to collect various imaging data.

Lovelace (2015) concluded the use of UAVs in bridge inspections are a safe method to inspect bridges, can provide detailed imagery of defects, and are a cost-effective tool to assist in inspecting bridges. Based on these conclusions, Lovelace recommended UAVs be used to assist bridge inspection teams.

Phase two of the demonstration project built on phase one with the goal to determine the ability of UAVs to inspect large scale steel bridges (Wells & Lovelace, 2017). The UAV inspections were compared with the current standards of hands-on inspections. The methods of inspection followed the same process as phase one as did the imaging devices used.

Based off the research in phase two, Wells and Lovelace (2017) concluded UASs are beneficial to assisting bridge inspectors for large scale bridges by providing ease of inspection to areas difficult to access, reducing costs associated with bridge inspections, and provide 3-D models of the bridge. Based off the conclusions of the research, Lovelace recommended UAVs for large scale bridges and where the risk to inspection personnel and the public are a concern.

2.3.4 Utah Department of Transportation

Barfuss *et al.* (2012) used a fixed wing UAV equipped with a high-resolution camera to monitor and document a highway construction project, and to capture digital RGB and near infrared images to classify wetland plant species. They found the high-resolution imagery provided UDOT with valuable information on construction progress, staging areas, and cut and fill areas as well as adding the historical records of the construction project. Barfuss *et al.* (2012) concluded the fixed UAV was most beneficial when UDOT required immediate imagery of Utah roadways and would benefit from the UAV imagery for classifying and monitoring wetland plant species.

2.3.5 Michigan Department of Transportation

Brooks *et al.* (2014) tested five sUAS with multiple image sensors to include high resolution camera, thermal, and lidar to monitor and assess transportation infrastructure. Team investigated the use of UAS to determine how the technology can assist MDOT personnel with visual inspections of a variety of infrastructure. Based on the tests and demonstrations the team provided recommendations and an implementation plan on the utilization of UAVs by MDOT. Brooks *et al.* (2014) concluded sUAS can help with transportation infrastructure monitoring.

2.3.6 Kansas Department of Transportation

McGuire *et al.* (2016) conducted research to provide a recommendation to KDOT as to whether the use of UAVs would be beneficial. A literature review was conducted to develop survey questions that were sent to other State Department of Transportation offices. Last the team conducted a strengths, weaknesses, opportunities, and

threats/challenges (SWOT) analysis. McGuire *et al.* (2016) concluded the use of UAVs by KDOT would improve safety, efficiency, and could reduce costs associated with inspections of bridges, radio towers, and high-mast light towers. They also found UAVs beneficial for surveying, road mapping, stockpile measurements, and aerial photographs.

2.3.7 Oregon Department of Transportation

Gillins *et al.* (2018) conducted tests to determine the feasibility of using sUAS to inspect bridges and communication towers. The study used six bridges and three towers to test the capabilities of using the sUAS for inspections. The study found sUAS well suited for assisting in the inspection of bridge decks, superstructures, and substructures. In particular, the study found sUAS capable of detecting cracks and other defects. Additionally, the study found sUAS can be very helpful in recording geometric data of the bridge through 3-D reconstruction. Furthermore, Gillins *et al.* (2018) concluded using sUAS in bridge inspections can save \$10,000 per bridge inspection.

These findings provide a foundation for further investigation into the use of sUAS in bridge inspection.

2.4 sUAS for Disaster Mitigation

UAV-RS has shown promise in identifying sites of potential disasters. A study conducted by Hu, Wu, and Tan (2012) successfully used UAS-RS in locating geological hazards along a pipeline in China – for example a landslide by tracing to its source of erosion and collapse. Information of potential landslides in the estimation stage of a project is crucial for accurate risk assessment and mitigation measures. Researchers have shown promise utilizing fixed wing and quadcopter UAVs outfitted with camera-based

platforms in detecting potential landslide areas (Carvajal, Aguera, & Perez, 2011; Rau, Jhan, Lob, & Linbet, 2011).

Damage assessments following natural disasters are daunting and arduous endeavors that are resources intensive, both in equipment and manpower. Current assessment methods have evolved from the traditional methods of personnel physically conducting detailed and rapid surveys of damage to utilizing unmanned aerial vehicles equipped with remote sensing technology (UAV-RS) in recent large-scale disaster events such as Hurricanes Harvey, Irma, Maria, and other disasters. “For rapid damage assessment, remote sensing has been found to be very useful, as it can cover large areas, and image-based assessments are realized more rapidly than through ground deployment of appropriately skilled surveyors”. In 2005 Pratt *et al.* (2006) conducted a National Science Foundation project to archive structural damage of six multiple story commercial buildings. The UAV-RS consisted of rotary wing unmanned vehicle equipped with a forward-looking camera, a gimbal mounted with video and FLIR as well as an imaging platform. Results from this study identified key technological issues associated with the UAV platform used. Issues identified included; the lack of obstacle avoidance technology, lack of semi-autonomous flight for accessing some sites, sensor coverage, and weather conditions such as wind and rain affecting the rotary wing UAV.

Following Hurricane Wilma, a UAV and unmanned sea -surface vehicle (USV) were used in tandem to inspect a bridge (Murphy *et al.*, 2008). Although the original object of the study was using both the UAV and USV to inspect the same bridge independently the study found the optimal use of the UAV in support of the USV as a visual guide for the USV traveling through the waterway beneath the bridge. The aerial

provided by the UAV afforded the USV pilot situational awareness minimizing the effects of GPS error and restricted line of sight (Murphy *et al.*, 2008). A later study by Murphy *et al* (2009) showed the effectiveness of the use the UAV prior to deploying the USV as a reconnaissance, effectively providing terrain analysis for the USV pilot to plot a course.

UAV-RS capability to creating a 3-D map following a natural disaster was shown to be an effective tool for assessing damage. Following the 2009 Typhoon Morakot, Taiwan received a large amount of rainfall in a short period of time, leading to severe flooding triggering massive mudslides. Chou *et al.* (2010) employed UAV-RS to collect imagery for assessing damage in support of recovery operations. The imagery provided by the UAV-RS team gave response and recovery officials a near real-time assessment of the affected areas for planning resource allocation. 3-D mapping using UAV-RS proved valuable following the Oso mudslide in March 2014. Precision-Hawk employed a fixed wing UAV-RS to create a detailed 3-D image of the terrain. The 3-D image provided by the UAV-RS gave geologist the information to predict the path of the mudslide and communicated these predictions with first responders along with the real time images to facilitate rescue and recovery efforts (Reich, January 2016). 3-D mapping capabilities provided by UAV-RS gives disaster response and recovery personnel the ability to represent the current conditions of the topography following disaster suppling response and recovery personnel the ability plan and allocate limited resources and inform local communities of impending dangers.

In 2016, a 7.8 magnitude earthquake struck Ecuador. Twenty-four hours after the earthquake, UAV-RS teams surveyed the damage providing first responders and local

officials with detailed 3-D images of affected area. These 3-D images provided by UAV-RS gave first responders the detailed representations of damaged building in affected areas where survivors needed aid (Duverneuil, 2016). UAV-RS ability to provided first responders and recovery personnel with real time visual information via 3-D images, increase their ability to effectively assign limited resources to locations based off facts obtained through the imagery of affected areas.

UAV-RS ability to access areas which are inaccessible to personnel, as was highlighted in the 2009 Typhoon Morakot, the Oso Mudslide in 2014, and the 2016 Ecuador earthquake. But in 2011, following the Fukushima Daiichi Nuclear Power Plant melt down resulting from the Tohoku earthquake and subsequent tsunami UAV-RS was tested in a radiation disaster. Response and recovery personnel deployed UAV-RS that was capable to register radiation levels while simultaneously visually inspect the damage (Duverneuil, 2016). The use of UAV-RS in and around the Fukushima Daiichi Nuclear Power Plant prevented exposure of personnel to radiation while enabling teams to assess damage, radiation levels, and monitor the path of radiation contamination. Obtaining reliable estimates from the UAV-RS equipped with radiation detection capability and high-resolution camera, reduced risk and avoided interruptions in assessing the damage by limiting the need for additional personnel to radioactive environment. UAV-RS ability to access a chemical, biological, radiological, nuclear, and explosive environment (CBRN-E) enables response and recovery operations enables accessibility to affected areas - regardless of contamination levels - for damage assessments and record levels of contamination.

Yamamoto *et al.* (2014) conducted an experiment using a UAV equipped with a digital camera and photogrammetry software to survey damage following a typhoon that severely damaged different regions in Japan. The photogrammetry software used was Photog-CAD which converted three 2D images into a 3D model and then converted model into a CAD drawing to assist in calculating construction cost.

In November of 2014 Bennett Industrial Landfill in Lockhart, S.C. was reported to be on fire prompting a response from county and state emergency management agencies due to the asbestos disposal cell and bags of asbestos containing material found throughout the landfill (EPA 2017). Because of the toxic particulates being released into the air and the active fire, ground surveyors were unable to conduct an accurate volumetric survey for the Environmental Protection Agency (EPA). The EPA decided to contract the use of a fixed wing UAV-RS to create a 3-D image of the site and conduct surveys obtaining volumetric quantities to facilitate a proper response (Reich, 2016).

Debris from hurricanes high winds, storm surge, and torrential rain cause further damage bridges and overpass. Damage to bridge and overpass can compromise their load bearing capacity and therefor impact vehicle access to areas requiring recovery. A reduction in load bearing capacity of a bridge or overpass causes safety and logistical implications for recovery and reconstruction teams by having to find alternate routes as for equipment and materials. UAV-RS is proven in the ability to assess damage to infrastructure such as bridges and overpasses.

A study conducted by Zhao and Ding (2005) found using traditional methods of assessing structural damage on bridges utilizing personnel and equipment is not only time consuming and expensive but is dangerous for inspectors. Traditional methods of

inspection require inspectors to go onto the deck structure and under the superstructure to inspect for damage, and the underside of the superstructure to inspect damage to the superstructure and the substructure. Following a disaster, traditional methods of inspecting bridge components increases the risk factors of safety for inspectors due to unknown damage to the deck, super, and substructure of the bridge as well as the subgrade supporting the substructure. UAV-RS is proven capable of conducting visual inspection with high resolution cameras, providing 360-degree assessment of bridges with limited exposure to personnel.

UAVs equipped with thermal imaging forward looking infrared (FLIR) for low visibility conditions to find source of ignition in fires and detecting heat in electrical power station and chemical plants to avoid a construction site catastrophe. Omar and Nehdi (2017) found UAVs equipment infra-red technology showed promise in reinforced concrete bridges. They confirmed the findings of the UAV-FLIR in detecting subsurface defects (delamination) by comparing results with traditional hammer sounding and half-cell potential tests conducted on the same bridge. Confirmation of the thermal imaging capability of UAVs show the potential in detecting potential hazards to construction workers and limiting risk of inspection teams.

UAV-RS serve as enablers in disaster response and recovery operations. The multitude of platforms available to mount on UAVs range from high optic cameras, light detection and ranging (LIDAR), FLIR, wi-fi routers, CBRN-E detection equipment, mapping sensors, and communication platforms (Duverneuil, 2016; Reich, 2016). UAVs offer another feature making them highly effective in post-disaster situations, semi-autonomous flight. UAVs can be preprogramed with a flight pattern using global

positioning systems (GPS) and software (Seibert & Teizer, 2014; Duverneuil, 2016).

Semi-autonomous flight allows multiple UAVs to fly on preprogrammed routes without the need for line of site operation.

Despite all the benefits, UAV-RS technology requires further study. Utilizing the myriad of UAV-RS technology in concert with multiple heterogeneous organizations to create a “common operating picture” will take collaboration and coordination between governments, non-government organizations, corporations, and communities. Through a collaborative effort UAV -RS technology can evolve to better support post-disaster recovery and reconstruction efforts by addressing local regulations, mitigate effects of extreme weather and limited battery (Duverneuil, 2016). The demand for UAV-RS technology in post-disaster recovery and reconstruction is apparent based on prior research in emerging UAV-RS technology. Reich (2017), highlights the rapid convergence and advancement of UAV-RS and other technologies provides practitioners with boundless opportunities to save time, money, and lives.

Several studies show UAVs equipped with a high-resolution camera can quantify material through photogrammetry (Carvajal *et al.*, 2011; Rau *et al.*, 2011; Siebert & Teizer, 2014; Duarte *et al.*, 2017; Vetrivel *et al.*, 2018). Photogrammetry affords UAVs the ability to visually represent the ground truth through 3-D models, making it a viable tool in assessing debris and infrastructure. Studies show flight path planning software and GPS allow UAVs to fly semi autonomously operating beyond visual contact of the operator, allowing for greater distances.

Although photogrammetry provides an ortho-photograph of the ground, limited visibility conditions (i.e. clouds, fog, and smoke), vegetation, and deep shadows inhibit

photogrammetry from establishing ground points, thus creating cavities in the image. Conversely dual sensor thermal imaging affords the ability see through limited visibility conditions (i.e. clouds, fog, and smoke), vegetation and deep shadows but lacks the real image capability provide by photogrammetry. Additionally, the research shows thermal imaging mounted on UAVs can detect delamination in concrete bridge decks with good degree of accuracy (Omar & Nehdi, 2017; Escobar-Wolf, 2017).

Therefore, this research seeks to harness a variety of UAV-RS technologies to facilitate a rapid assessment of highway and road infrastructure. The amalgamation of photogrammetry, dual sensor thermal imaging, coupled with semi-autonomous flight capability of UAV-RS provides practitioners the ability to begin immediate assessments of debris and infrastructure along highways and roads with a high degree of fidelity. The proposed research seeks to validate the capabilities of UAV-RS in assessing a critical highway infrastructure component (steel bridge girders) to reduce uncertainty of the status of a steel bridge in the early parts of recovery. The purposed this research of UAV-RS in assessing damage and defects to steel bridge girders is part of a system of systems to predict viable routes for recovery and egress operations.

2.4 Chapter Summary

A review of the literature above demonstrated the use of UAV-RS following a disaster event. A key component of successful disaster recovery is the ability access road infrastructure. As noted by the studies in the literature review, sUAS have a positive impact with disaster response and recovery by providing information about the extent of disasters to quickly assess the situation on the ground. However, the studies show a lack of knowledge in developing the ability to detect damage and defects in steel bridge

components during low-light conditions. Furthermore, there is a lack of knowledge on the capabilities of UAV-RS to assess the type of damage and defects in low-light conditions.

This research was influenced by the previous studies in UAV-RS applications in construction and disaster recovery showing the capabilities of UAV-RS in construction and disaster recovery but sought to expand the knowledge in qualifying the type of damage and defects to steel bridge components in low-light environments. By testing the combined capabilities of RGB low-light and thermal imaging camera the research sought to determine UAV-RS ability to conduct an assessment of damage and defects to steel bridge girder in low-light conditions.

CHAPTER 3. FRAMEWORK AND METHODOLOGY

Chapter three provides detailed information on the framework, equipment, and methods used to test the sUAS ability to inspect steel bridge components in low-light conditions. The chapter begins by describing the framework followed by the equipment used in the experiments. The methodology begins by describing the materials used in the research and how the materials were selected. Second, the methods section describes the research protocol outlining sequence of the manipulations and measurement procedures making up the experiment. Third, the data collection section describes how the data was collected. Last, the data analysis section described how the data was presented in the results section of the research.

3.1 Framework

This research was based on an experimental design to ascertain the capabilities and limitations of a sUAS for inspecting steel bridge components in low-light condition. A small hex-copter sUAV equipped with a dual sensor camera (i.e. thermal imaging and RGB low-light) and a methodology was developed to evaluate the sUAS ability to inspect steel bridge components during low-light conditions. The methodology developed to determine the ability of using the sUAS in low-light conditions consisted of a series of experiments during nautical and astronomical twilight, and night conditions. The intent of the research was to determine if the technology is viable for inspecting structural damage in steel bridge members during low-light conditions.

The research approach utilizes an experimental procedure using a sUAS consisting of a dual sensor thermal and lowlight RGB camera attached to a three-axis gimbal. The sUAS are off the shelf and readily available. The overall process is:

- 1) Conduct an initial test flight of the sUAS to ensure the sUAV, dual sensor camera (thermal and RGB low-light camera), ground control station and flight path planning software system are operating as designed.
- 2) Identify steel girder(s) with structural defects to determine the level of reliability of the technologies to detect global defects in the steel girders in low-light conditions.
- 3) Conduct initial field test to determine the capability of the sUAS optics to obtain imagery of global defects in steel girders in low-light conditions.
- 4) Conduct experiments on the effects of low-light conditions at known distances on imagery of global defects in steel girders.
- 5) Validate the appropriate distance for obtaining imagery during low-light conditions of global defects in steel girders.

3.2 Equipment

3.2.1 Selection of Small Unmanned Aerial System

There are several commercially available UAS capable of surveying and conducting inspections. After a review of the literature, the evaluation criteria for selecting the sUAS required for inspecting steel bridge components in low-light conditions are as follows;

- 1) UAS capable of at least 20 minutes of flight time;
- 2) Camera system able to capture images in low-light conditions without an artificial light source;

- 3) A stabilized gimbal capable 90-degree pitch and 360-degree pan;
- 4) Capable of semi-autonomous flight;
- 5) Stable flight during windy conditions;
- 6) First-person view capability.

The evaluation criteria for dual sensor cameras was a lightweight small dual sensor camera capable of being mounted to gimbal on a quad, hex, or octocopter UAV. The dual sensor camera needed to be compact, lightweight, multi sensor system with high resolution, capable of panning 360 degrees with 180 degrees tilt, and capable of withstanding adverse conditions following a disaster. The purpose for the 360-degree panning and 90 degrees of tilt is to maximize the fields of view for inspection of bridges.

3.2.2 Small Unmanned Aerial System

The sUAS selected based off the criteria was the Yuneec H520 hex-copter equipped with the CGOET dual sensor camera with integrated gimbal (Figure 2). The UAV-RS system is capable of up to 28 minutes flight time with a thermal imaging and a low light camera with an integrated 3-axis gimbal, capable of a continuous 360-degree panning. The RGB low-light camera is 20 times more sensitive than the human eye, increasing the night vision capability of the camera. The sUAS come with a ground control station with a seven-inch multi-function display tablet that is Android-based and displays video, stills, telemetry, altitude, airspeed, location, number of satellites acquired, camera mode, and other information directly on the surface of the ground station controller and records and stores flight data. The ground control station has flight path planning software that allows for semi-autonomous flight.



Figure 2: Yuneec H520 UAV, CGOET camera, and ST16S ground control station.

3.2.2.1 Small Unmanned Aerial Vehicle

The Yuneec H520 is a six-rotor UAV capable of withstanding winds up to 48 kilometers per hour. The flight time per battery is approximately 28 minutes and the batteries can be changed during a mission greater than 28 minutes without losing data or memory of the programmed mission. During a mission greater than 28 minutes the H520 will return to launch site where the battery is changed and then returns to the point of departure and completes the mission. The H520 has obstacle avoidance capability using sonar. The specification of the UAV is shown in Table 1.

Table 1: Yuneec H520 UAV specifications

Specifications	UAV
Flight Time	Up to 28 min.
Battery	LiPo 5250mAh
Max. Horizontal Speed	17 m/s
Max. Climbing Speed	4 m/s
Max. Descending Speed	2.5 m/s

3.2.2.2 *Small Unmanned Aerial Vehicle Optics*

The camera was an integrated 3-axis gimbal, thermal imaging and lowlight RGB camera. The RGB lowlight 1080p RGB and thermal imaging camera provide a picture-in-picture overlay with dual-stream recording enabling separate editing of images, video or photographic. The camera is fully integrated with the sUAV and the ground control station (ST16s) and has a micro-SD port to save imagery obtained from the camera. The full integration allows the camera to bind to the ground control station and images to be streamed directly to ground control station. The specifications for the camera system are shown in Table 2.

Table 2: CGOET camera specifications

Specifications	RGB Lowlight	Thermal Imaging
Focal Length	23mm	
Video Resolution	1920 x 1080 30 fps	160 x 120 9 fps
Sensor	1/2.8" 2.13 MP	
ISO Range	100-12800	
Field of View (Diag.)	90°	71°
Field of View (Horiz.)		56°
Sensitivity		< 50mK
LWIR		8 - 14 μ m
Temp. Measuring Range		-10° to 180°C
Operating Temp. Range		-10° to 40°C

3.2.2.3 Small Unmanned Aerial Vehicle Ground Control Station

The ground control station was a transmitter and receiver with a 17.78cm screen which provides real-time telemetry data during flight operations and is an Android based tablet provides real-time footage from the camera. The screen displays flight mode, altitude, ground speed, distance from take-off location, camera status, GPS position coordinates, and battery status of UAV and ground station. The ground station enables pilots to control camera and video settings during flight and can share the image on a large monitor via HDMI cable.

The ground station was equipped with a flight planning software that is fully integrated with the hardware and software of the UAV system. The flight planning software system enables for the creation of orthomaps, 3D scans, and data imagery. Up to 500 waypoints can be plotted in a mission, each with a designated altitude, speed, and hold time. The camera options for each waypoint are; take photo, take photo (time), take photo (distance), stop taking photo, start taking video, and stop taking video. The specifications of the ground station are listed in Table 3.

Table 3: ST16S ground control station.

Specifications	ST16s Ground Station
Operating System	Android
Number of Channels	16
Transmission Dist.	1.6 km
Video Resolution	720p
Video Frequency	5.8GHz Wi-Fi
Video Transmission	1.6 km
Battery (built-in)	3.6V 870mAh 31.32Wh Li-ion
Connections	1x HDMI, 2x USB, 1x headphone

3.2.2.4 Flight Mode for Experiments

Angle flight mode was used in all experiments involving the sUAS. Angle flight mode is GPS assisted flight which enables stable flight. GPS assisted flight allows the UAV to hover in place when the pilot releases the thrust control. While in angle flight mode UAVs thrust, yaw, pitch and roll are relative to the front nose of the UAV. Furthermore, the degree of the angle of the aircraft is determined by how far the pilot moves the control stick from its center position. The two rear LED lights will be purple during angle flight mode, further assisting the pilot during low-light conditions as to the UAVs orientation. Angle flight mode was chosen for the experiments in this research due to the stability GPS assisted flights offer. This allowed the pilot to focus on capturing imagery necessary for analysis.

3.3 Experiment Methodology

3.3.1 Procedure for sUAS Steel Bridge Component Experiment

The experiment consisted of seven primary steps to conduct low-light inspections of damage to steel bridge components using UAS: 1) Selection of steel bridge components for experiment; 2) Experimental process; 3) Plan flight operations; 4) Conduct a preliminary flight; 5) Collect remote sensing data for analysis; 7) Perform analysis of remote sensing data.

3.3.2 Selection of Steel Bridge Components

Bridges are critical piece of road infrastructure and assessing them for damage following a disaster necessary. This is due to damage sustained to a fracture critical member, “fracture critical member (FCM) is steel member in tension, or with a tension

element, whose failure would probably cause a portion of or the entire bridge to collapse” (NBIS, 2012). Before crossing a bridge following a disaster, knowledge as to whether the load classification of the bridge has been compromised is essential in preventing a collapse. For this reason, assessing bridge damage is include as a variable in route optimization.

The number of structurally deficient steel bridges throughout the United States is 30,468 (Farhey, 2018b) and account for sixty five percent (65%) of bridge failures in the United States, with girders accounting for fifty eight percent (58%) of the structural type in bridge failures (Lee *et al.*, 2013). Furthermore, structural deficiencies for girder bridges in above the average for all other bridges by approximately three and half percent (3.5%) (Farhey, 2018a). Therefore, the research focuses on steel girders. S-BRITE laboratory is an outdoor facility that provides samples of steel bridge members with various degrees of damage, from minor defects to global damage.

A site visit to the S-BRITE facility aided in identifying steel bridge girders for the experiments. The S-BRITE laboratory at Purdue University had an assortment of steel bridge components in a control environment. Control environment is defined as one free from traffic, pedestrians, and other impediments (i.e. overhead electrical lines, buildings, and trees) to UAV operations. For these reasons, S-BRITE was selected as an ideal location for the experiments.

3.3.3 Experimental Process

The sUAS was used to collect remote sensing imagery of the selected steel bridge girders from the S-BRITE facility. The three phases of the experimental process: 1) initial test flight; 2) preliminary field test; 3) establishing the effects of low-light conditions (i.e.

nautical twilight, astronomical twilight, and night) and distance for observation of steel bridge components; 4) Validate.

3.3.3.1 Initial Flight Test

The purpose of the initial flight test was twofold; 1) For the pilot to become familiar with the flight characteristics of the UAV and 2) To ensure the UAV, lowlight and thermal camera, gimbal, ST16S ground station are operating correctly. During the initial flight test, the UAS pilot became familiar with the flight characteristics and the operation of the low-light RGB and thermal camera.

Prior to any flight operations, UAS pilot checked for updates to firmware and software, and ensures batteries and the base station are fully charged. When updates were available, they were downloaded and installed to the appropriate system – UAV, camera, gimbal, or base station. After updates were installed, preflight checks were conducted. Telemetry with the camera was checked on the base station and tests run on camera tilt, pan and the imagery settings. Satellite acquisition was confirmed on the base station and the battery power for both base station and the sUAS were displaying fully charged. Figure 3 was the flow chart followed prior to each experiment.

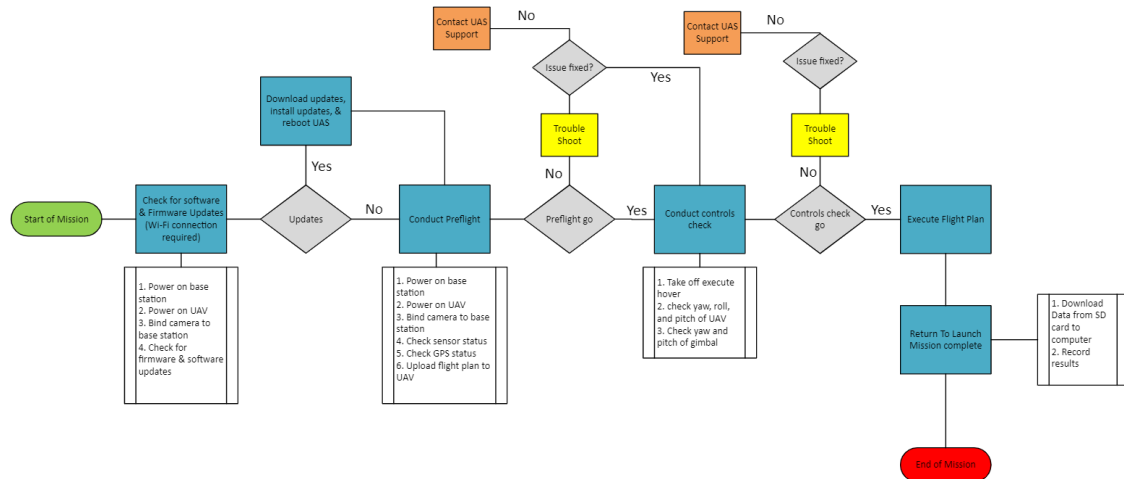


Figure 3: sUAS flight controls flow chart prior to each experiment.

3.3.3.2 Preliminary Field Experiment

A preliminary field test was conducted at the S-BRITE facility on Purdue University grounds under controlled conditions. The initial field experiment of the sUAS at the S-BRITE facility was to determine the capabilities of the thermal imaging and RGB low light camera in visually detecting known damage in steel bridge members. The bridge components in the initial field test were selected from the S-BRITE center. A section from each girder with visible damage was selected and recorded. The distance from the girders was four feet and hovering parallel to the girders to obtain the remote sensing imagery (thermal and low-light). For the thermal images, differing color pallets were used. The objectives of the preliminary filed experiment were:

- Determine the best thermal imaging color pallet for visually detecting damage in steel bridge members.
- Evaluate the capabilities and limitations of the thermal imaging camera and the RGB lowlight camera during nautical twilight.

- Evaluate the difference in visually detecting damage in steel girders between thermal imaging and RGB lowlight camera.
- Evaluate the capabilities of thermal imaging and RGB low-light camera as an inspection tool for steel bridge inspection during low-visibility condition.

The preliminary field tests were conducted during evening nautical twilight.

Evening nautical twilight is the end of nautical twilight where the center of the sun is geometrically 12 degrees below the horizon. During nautical twilight, the general outlines of ground objects may be distinguishable, but details are not (USNO, 2018). Due to the inability to ascertain details, nautical twilight was deemed appropriate for the preliminary field test of the UAS during low-light conditions.

3.3.3.3 Low-Light Inspection Distance Experiment

Following the preliminary field test, an experiment to determine a suitable distance from the steel girder was conducted at the S-BRITE facility. The third step in the experiment was to establish how low-light conditions and distance effects the sUAS ability to capture imagery of damage and defects on the steel girder. After the baseline was established for the steel girder the sUAS was flown at varying distances using both RGB low-light camera and the thermal imaging camera capturing imagery of damage and defects in the steel girder under low-light conditions. The altitude, distance from the steel girder, air temperature, time of day, and ability to observe damage and defects in the imagery of the low-level camera and thermal camera was recorded. Two key factors that gives steel a higher emissivity of is roughness and oxidization (Mikron) both of which are

present in damaged areas of steel exposed to elements. Based on this fact the thermal camera was predicted to be able to detect damage and defects in the steel girder.

To determine the effects of low-light conditions on detecting damage and defects in the steel girder, the experiment was conducted during evening nautical twilight, evening astronomical twilight, and night. Evening astronomical twilight is where the center of the Sun is geometrically 18 degrees below the horizon and the illumination in the sky is practically unnoticeable (USNO, 2018). After the end of evening astronomical twilight, when the center of the Sun passes 18 degrees below the horizon, the light from the Sun is less than that from the starlight, which is considered night.

First, cones were placed at known distances from the steel deck girder plate, perpendicular to the damage and defects in the web. The cones served as markers at known distances from the web for the UAV pilot to hover and capture imagery of the web. The distances were measured from the web using a standard 25-foot (7.62m) tape measure beginning at four feet (1.22 m) from the web and placing cones every two feet (0.61m) thereafter up to 20 feet (6.1m). Figure 4 is a pictorial representation of the layout for the experiment.

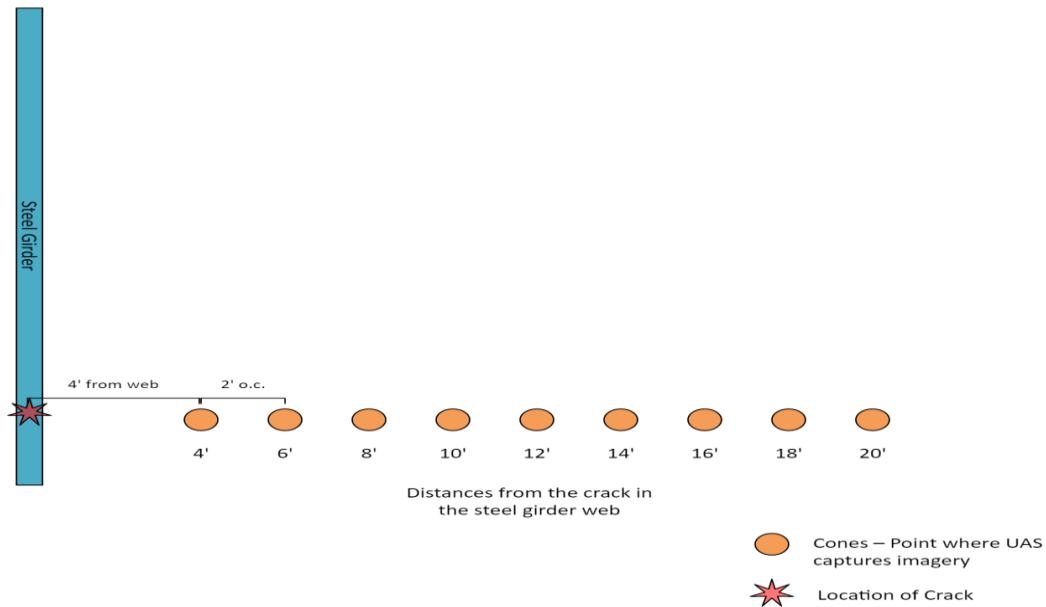


Figure 4: Low-light distance experiment diagram.

Following the experiment imagery data was downloaded from the micro-SD card to the computer for analysis. Figure 5 shows the flow chart for the steel girder experiments.

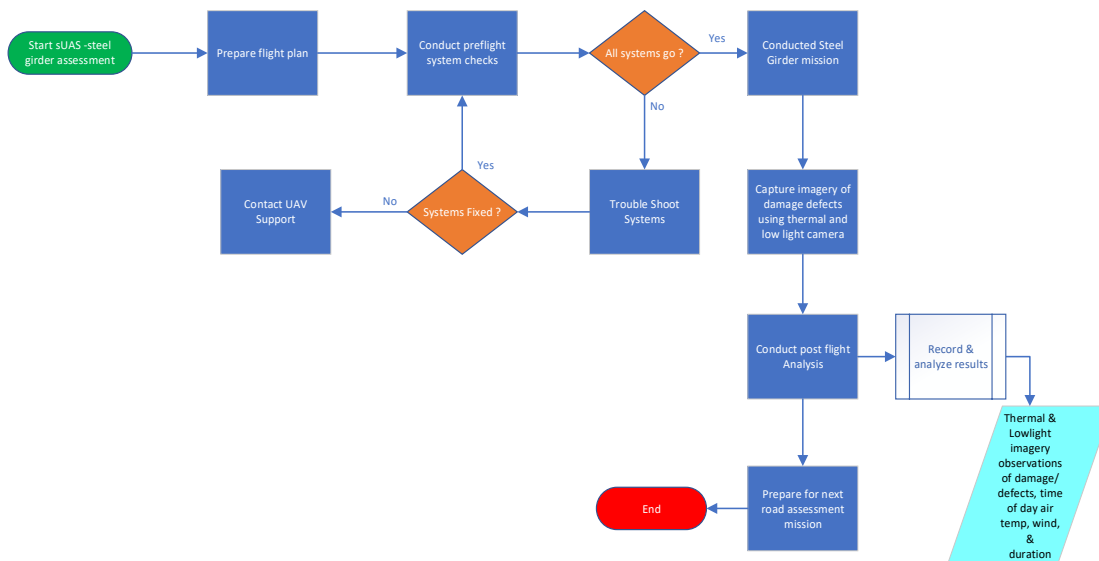


Figure 5: Steel Girder experiments flow chart

3.3.3.4 Validation Distance Experiment

Following the low-light inspection distance experiment, an experiment to validate the suitable distance determined from the low-light distance experiment was conducted. This part of the experiment was based on the results from the low-light distance experiment for all three low-light conditions. Cones were placed at a suitable distance from the Virginia Ave steel girder to observe damage and defects and parallel with the girder (Figure 6). These cones served as a flight path for the sUAS pilot to test if the distances obtained in the previous experiment are sufficient to observe damage and defects in the steel girder.

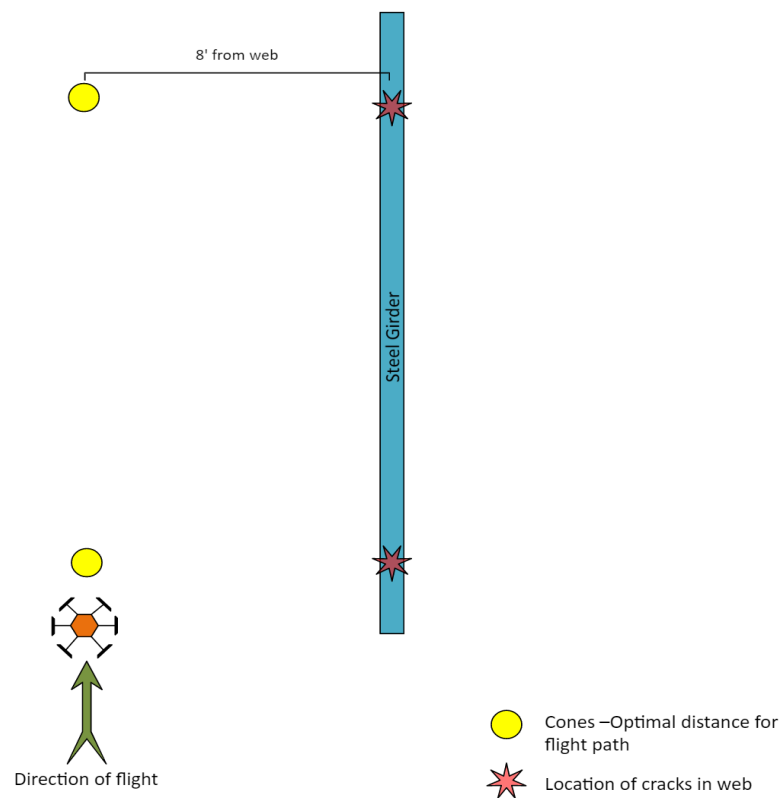


Figure 6: Validation experiment diagram.

3.4 Unit of Analysis

The unit of analysis was the imagery of damage and defects obtained of the steel bridge girder via the sUAS RGB low-light and thermal imaging camera. Each image was analyzed based on the ability to visually observe damage and defects. These images were used to analyze the capability of the RGB low-light and thermal imaging camera to observe steel bridge girders for global damage in low-light conditions.

3.5 Data Collection

Imagery was captured by the sUAS thermal imaging and RGB low-light camera. Both photographic and video imagery was captured by the thermal and RGB low-light camera. The sUAS camera has a micro-SD port where a 16-megabit micro-SD card is located. All photos and video from the test flights were store on the micro-SD card. A Surface Pro 4 was used to view photos and video from the micro-SD card. After each experiment the imagery was download off the micro-SD card and saved for analysis. Imagery data was collected over a series of experiments spanning several months. The imagery obtained from the experiments provides data for analysis in this research and provided a basis for further studies.

3.6Threats to Validity

Existing steel bridge members at the S-BRITE facilities were good for collecting data for the research, but external factors such as weather cannot were not controlled during the experiment and as such may have influenced the imagery captured. The sUAS had several updates to the software and firmware which may have affected the flight characteristics and optical sensors between experiments. The experiment was only

conducted in the state of Indiana and therefore was subject to environmental conditions of Indiana.

3.7 Data Analysis

Each experiment collected imagery data during evening nautical and astronomical twilight, and night establishing the effects of differing low-light conditions on the imagery collected by the sUAS. Additionally, the distance experiments tested whether there was a correlation between low-light, distance, and the detection of defects in steel bridge members. The multiple experiments provided imagery data variability over differing low-light conditions. This variability in low-light condition was used to answer the research questions.

For the first research question, what is the effect of low-light conditions on the sUAS optics to assess global structural damage and defects, and the second research question, what effect does distance in low-light conditions have on the ability to observe global structural damage, the imagery obtained was used to examine the global damage and defects visible during nautical and astronomical twilight and night at known distances. This information was used to validate a suitable distance range to observe global damage and defects in steel bridge girders.

3.8 Chapter Summary

Chapter three covered the framework and methodology of the scientific investigation in use UAV-RS in post-disaster damage assessment and debris estimation during low visibility conditions. Furthermore, the chapter covered how the data was

collected and analyzed and supplied the model to determine the optimal distance to observe damage ad defects in bridge steel members.

CHAPTER 4. DATA ANALYSIS AND RESULTS

This chapter presents the results and analysis of the data collected using the methodology and equipment discussed in the previous chapter. The data was collected using the sUAS and then analyzed in response the three research questions:

1. What is the effect of low-light conditions on the sUAS optics to assess global structural damage?
2. What effect does distance have on the sUAS camera imagery in observing damage and defects in the structural steel during low-light conditions?
3. What is the logical correlation, if any, between the sUAS camera imagery to observe damage and defects during low-light conditions at a given distance?

This chapter will first provide a summary of each of the steel bridge member experiments followed the analysis of each experiment.

4.1 Initial Flight Test

The initial flight test was conducted at Bowen Laboratory outdoor testing yard (Figure 7). The outdoor testing yard has an area of 82,000 square feet providing ample space to conduct the initial flight test. The following preflight procedures were conducted: 1) selection of suitable takeoff and landing site free of personnel, equipment, and obstacles; 2) power on the base station; 3) power on the UAV; 3) bind camera to the base station; 4) calibrate compass, accelerometer, and gimbal; 5) place UAV at launch site in angle flight mode and arm UAV. Once the UAV was armed, a hovered at 20 feet was executed to check the telemetry of the controls: pitch, yaw, and roll of UAV and the

yaw and pitch of the camera mounted gimbal. The UAV was then flown around the yard using the camera system the color schemes of the thermal camera on steel I-beam.

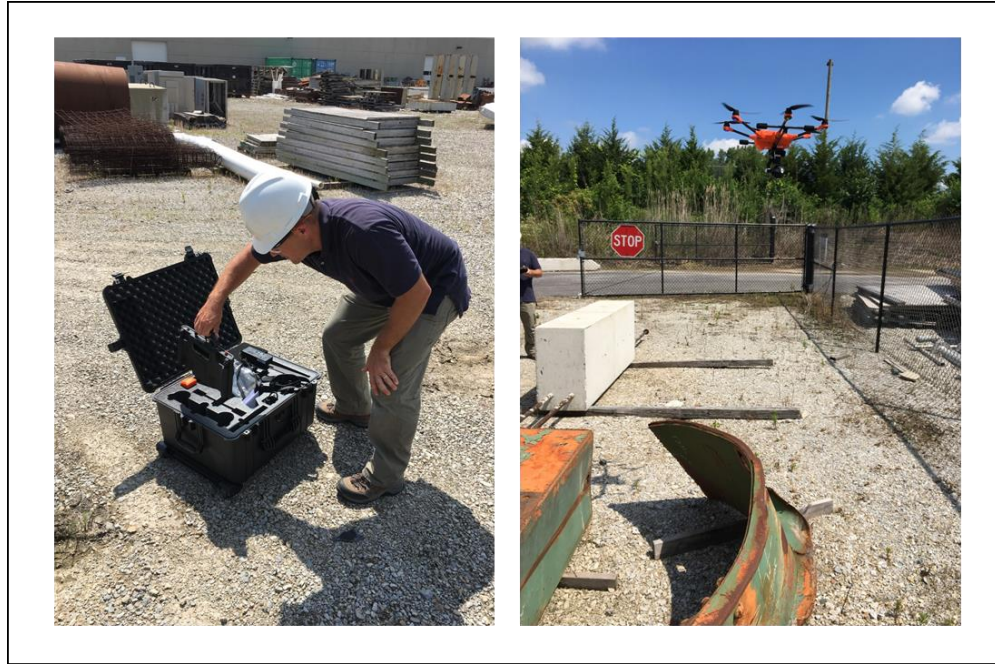


Figure 7: Bowen Laboratory initial flight test.

4.2 Visual Data of sUAS Imagery

4.2.1 Preliminary Field Test of Steel Bridge Members at S-BRITE

The preliminary field test was conducted at the S-BRITE facility on Purdue University grounds under controlled conditions. The S-BRITE facility was chosen due to the availability of steel bridge members in an outdoor environment. The first steel girder, bridge span D234 (a) in figure 8 from the Norfolk Southern Railroad (NSR), had multiple holes in the web near the bottom flange. The span is 40 feet in length from Rockfield, Indiana and was the main span of the three-span structure totaling 112 feet and 10 inches. The span has multiple sections with loss of web plate and a missing rivet from the

original construction. The steel girder was supported by two concrete blocks at either end of steel girder approximately 54 inches (1.37 m) off the ground. Due to the visual damage, this girder was selected for the experiments.

The second steel girder (b) in figure 8 from the Virginia Avenue Bridge, had two complete cracks in the web. The Virginia Avenue Bridge was a single span of 155 feet and carrier traffic over I-65/I-70 in Indianapolis, Indiana. The north bound fascia deck girder section used in the test was fractured from a truck collision in February 2013. The fracture necessitated emergency repairs (mending plates secured over the fracture) prior to being replaced later in 2013. The damage used for the initial study was recorded prior to conducting the study and is used to validate the results.



Figure 8: Steel bridge members at S-BRITE: (a) Norfolk Southern Railroad deck plate girder span; (b) Virginia Avenue bridge girder.

Prior to beginning the first field experiment, a suitable launch site was selected in the vicinity of the two girders and preflight procedures were executed. The UAV was flown approximately 4 feet (1.22 m) from the steel girders hovering at an altitude of 5 feet (1.524 m). Imagery from the remote sensor was captured using the rainbow and

white-hot color schemes, and the low-light RGB camera for analysis. The remote sensing platform for the initial test was the thermal imaging and RGB lowlight camera mounted on the bottom of the UAV with stabilizing 2 axis gimbal.

The sUAS was used in the preliminary test to collect image data of damage on steel bridge girders during low-light conditions. The preliminary field test was conducted on Purdue University grounds under controlled conditions at the S-BRITE facility during nautical twilight. The preliminary test of the sUAS conducted at the S-BRITE facility was to ascertain the capabilities of the thermal imaging and RGB low light camera in visually detecting known damage in steel bridge members. The objectives of the test were to:

- Determine the best thermal imaging color pallet for visually detecting defects in steel bridge members.
- Evaluate the capabilities of the thermal imaging camera and the RGB lowlight camera during EENT.
- Evaluate the difference in visually detecting damage and defects in steel girders between thermal imaging and RGB lowlight camera.
- Evaluate the capabilities of thermal imaging and RGB lowlight camera as an inspection tool for steel bridge inspection post-disaster.

For this research, the camera system was set to capture still photographs with the display mode on the base station screen set to full for displaying only infrared images. The color pallets selected for the initial field study were rainbow and white hot. Rainbow color pallet was chosen due to the greater number of colors used to discern the temperature ranges of infrared heat emitted by the steel girder. The white-hot color pallet

was also chosen for the ability to distinguish the temperature differential of infrared heat emitted by identifying high heat signatures with white and cooler areas with black.

The preliminary field tests were conducted on July 24, 2018 at 9:42 pm during evening nautical twilight. The temperature range for July 24, 2018 was 86 degrees Fahrenheit (30 Celsius) for the high and 66 degrees Fahrenheit (19 Celsius) for the low. Air temperature at the time of the test was 79 degrees Fahrenheit (26 Celsius) – a seven-degree Fahrenheit temperature differential - with a relative humidity of 60 percent. Winds were out of the northwest (350) at 4 miles per hour. The following sections provide the results of each field test.

4.2.1.1 Preliminary Field Test - Norfolk Southern Railroad (NSR) Deck Girder Span

The NSR deck girder plate was the target of the first field test for the thermal imaging and lowlight camera on Purdue University's S-BRITE facility. The noticeable visual defects made the D234 span the focus of the first field test for the thermal imaging and low light camera. The section used in the preliminary field experiment was 0.748 inches (19 mm) in diameter and was recorded prior to conducting the experiment.

The remote sensing platform for this test was the thermal imaging and RGB lowlight camera mounted on the bottom of the UAV with stabilizing 3 axis gimbal. The sUAS captured the images from approximately four feet (1.22m).

The section used in this study was 3/4 inches (19.05 mm) in diameter. The steel girder was supported by two concrete blocks at either end of steel girder. The steel girder was 54 inches (1.37 m) off the ground. The damage used for the initial study was recorded prior to conducting the study and is used to validate the results.

Figures 9, 10, and 11 capture defects found during the field test on the NSR steel girder span D234. The images capture a section loss in the web plate and the severe amount of rust chips from the web plate.

Figure 9 is captured from the RGB low-light camera. The 0.748 inches (19 mm) hole in the web plate is easily identified as are the rust chips. The RGB low-light camera image provides high resolution detail of the steel girder. The angle plate and rivets used to reinforce the joint between the web and flange are easily discerned. The level of oxidation of the steel girder is seen clearly in the image.



Figure 9: RGB low-light camera image of 0.748-inch (19 mm) hole in web steel girder span D234.

Figure 10 is a thermal image of the same section of NSR steel girder span D234 obtained using the RGB low-light camera. The thermal imaging color pallet used in Figure 10 is rainbow. In the rainbow thermal image, the rust chip is easily identified but the section loss in the web plate is more difficult to identify. This may be due to the angle

the image was captured. The angle plate and rivets used to reinforce joint between the web and flange are identifiable. The areas of oxidation appear yellow (i.e. hotter) and areas less oxidized appear green (i.e. cooler).

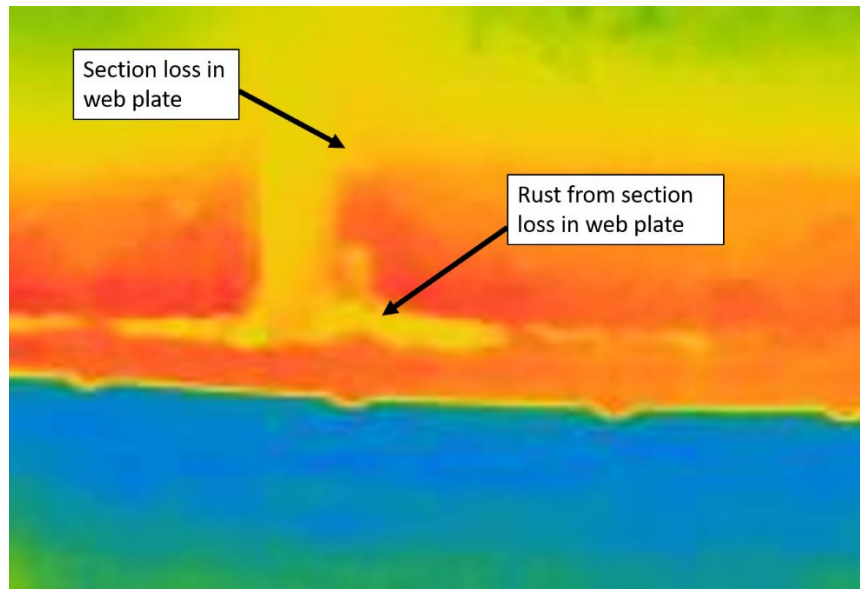


Figure 10: Thermal image of 0.748 inch (19 mm) in web of NSR steel girder span D234 (rainbow pallet).

Figure 11 is a thermal image of the same section of NSR steel girder span D234 obtained using the RGB low-light camera and rainbow thermal imaging color pallet. The thermal imaging color pallet used in Figure 11 is white hot. This color pallet was chosen for a black and white representation of the steel girder. In the white-hot thermal image, the rust flakes are easily identified due to the rust flakes having a lower temperature than the steel girder. The section loss in the web plate is cannot be discerned at this angle from the rest of the web. The lack of discernibility may be a result to the resolution of the thermal camera and angle the images was obtained.

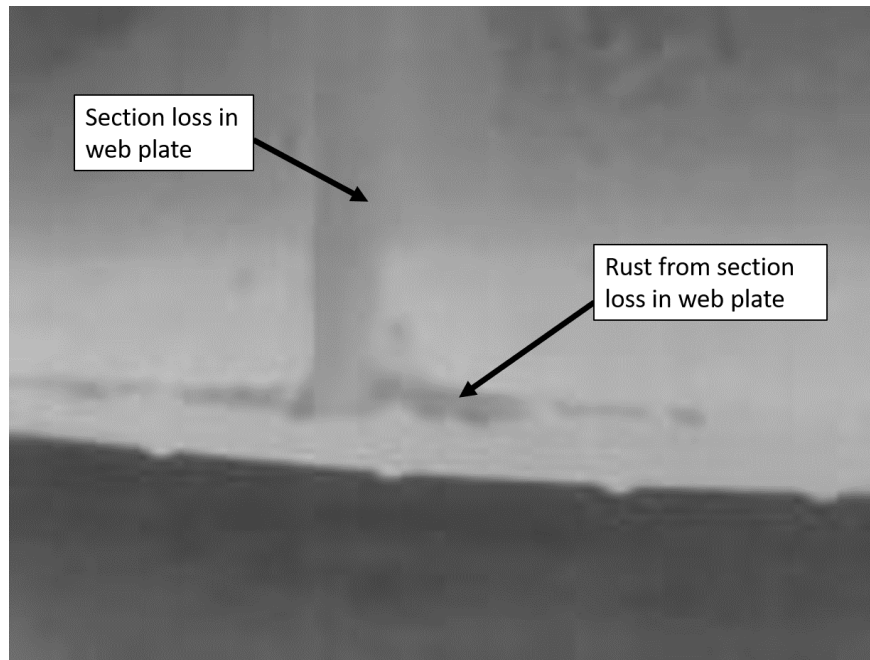


Figure 11: Thermal image of 0.748-inch hole in web of NSR steel girder span D234 (white hot pallet).

4.2.1.2 Preliminary Field Test – Virginia Avenue Bridge

The Virginia Avenue Bridge deck girder plate from was the second target of the first field test for the thermal imaging and lowlight camera at Purdue Universities S-BRITE facility. The fracture in the web with mending plates made the north bound girder the focus of the first field experiment for the thermal imaging and RGB lowlight camera.

The remote sensing platform for this test was the thermal imaging and RGB lowlight camera mounted on the bottom of the six-rotor UAV with stabilizing 3-axis gimbal. The distance images were obtained by the sUAS from the Virginia Avenue Bridge's north bound steel girder was four feet (1.22m) at an altitude of approximately 5 feet 6 inches (1.68m) above ground level. This altitude placed the UAV approximately perpendicular to the center of the web.

The crack in the web for the initial study is 0.039 inches (1 mm) wide between mending plates one and two, 0.079 inches (2 mm) between mending plates two and three, and 0.138 inches (3.5 mm) below mending plate three. The crack in the web is 57 inches (1.45 m) in length, with the total length of the web at 59 inches (1.5 m) from the bottom flange to the top flange. The crack begins approximately 2 inches (5.08 cm) from the top flange and extends vertically through the web down to the bottom flange of the steel girder.

Figures 12, 13, and 14 capture defects found during the field test on the Virginia Avenue Bridge north bound steel girder. The images capture a fracture in the web plate and the mending plates for the fracture in the web plate.

The image of the north bound girder, Figure 12 is captured using the RGB low-light camera. All three cracks; 0.039 inches (1 mm) wide between mending plates one and two, 0.079 inches (2 mm) between mending plates two and three, and 0.138 inches (3.5 mm) below mending plate three, in the web are easily identified as are the mending plates and bolts. The lowlight camera image provides additional details of abrasion in the lower left of the image that is evidence of the girder being struck by an object.

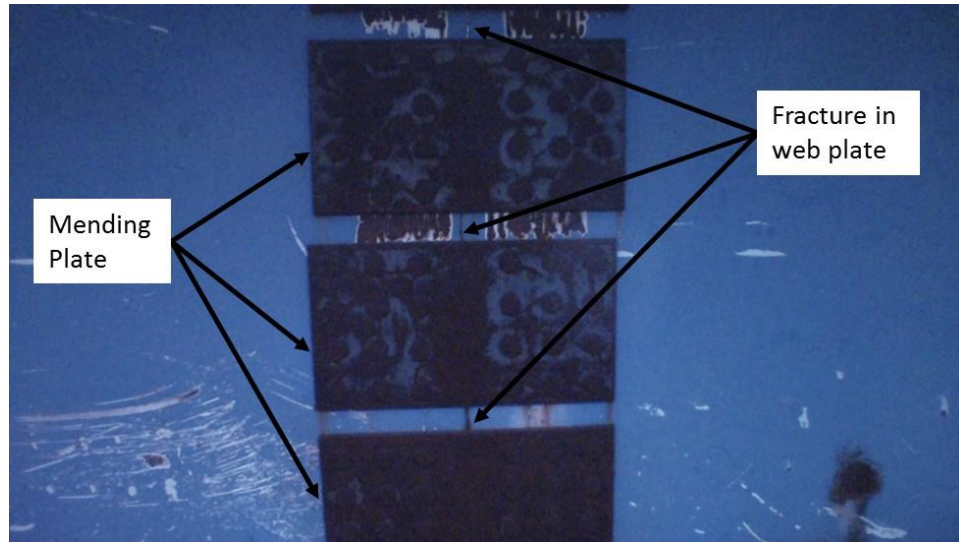


Figure 12: RGB low-light image of crack in web of Virginia Avenue bridge steel girder.

Figure 13 is a thermal image of the same section of Virginia Avenue Bridge's north bound steel girder obtained with the RGB low-light camera. The thermal imaging color pallet used in Figure 13 is rainbow. This color pallet was chosen due to the greater number of colors used to discern different temperatures of infrared heat emitted by the steel girder. In the rainbow thermal image, the repaired area is easily identified from the rest of the steel girder but the fracture in the web plate not distinguishable.

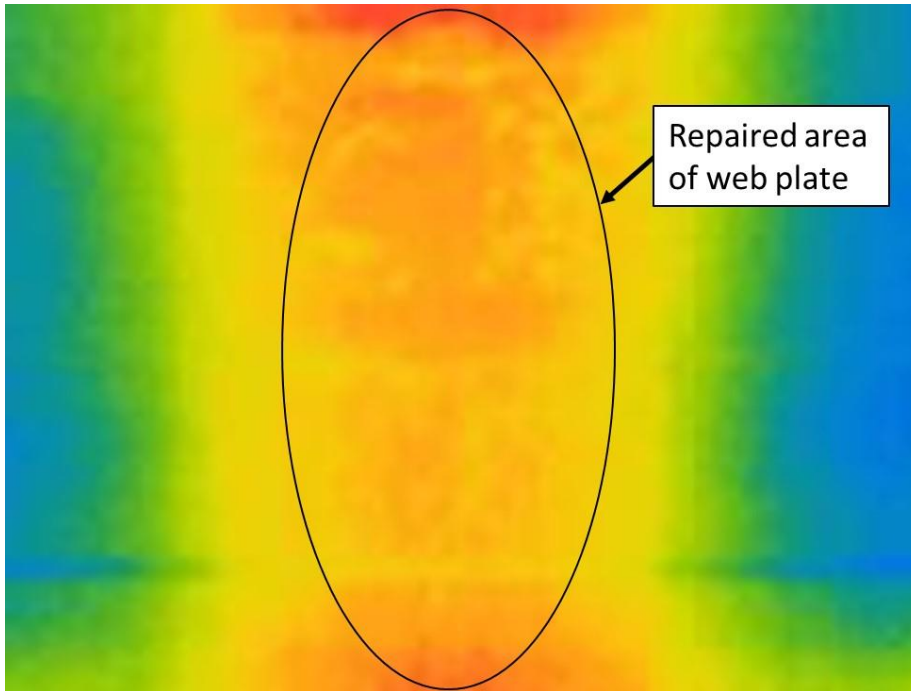


Figure 13: Thermal image of crack in web of Virginia Avenue steel girder (rainbow pallet).

Although the fracture in the web plate is not discernable, the area of damage is discernable. Note the cooler blue area to the left and right of the fracture area, these areas have a coating of gloss paint (lower emissivity) and the repaired area has rough steel mending plates (higher emissivity). Additionally, the larger crack, 0.138 inches (3.5 mm), below mending plate three is faintly noticeable. The image shows the painted area radiates energy less than the areas where there is no paint.

Figure 14 is a thermal image using a different color pallet of the same section of Virginia Avenue steel girder span obtained using the RGB low-light camera and rainbow thermal imaging color pallet. The thermal imaging color pallet used in Figure 14 is white hot. This color pallet was chosen for a black and white representation of the steel girder. The white-hot color pallet distinguishes the temperature differential from the infrared

heat emitted by identifying high heat signatures with white and cooler areas with black. In the white-hot thermal image, the mending plates are easily identified along with most of the bolts but the fracture in the web plate is not discernable from the rest of the web.

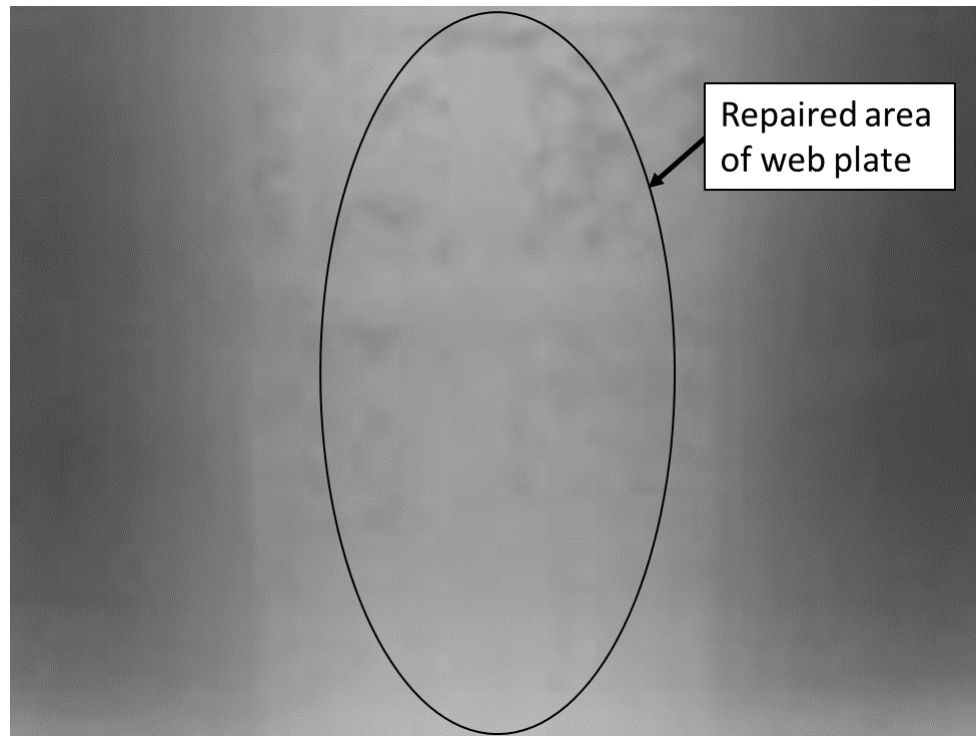


Figure 14: Thermal image of crack in web of Virginia Avenue steel girder (white hot pallet)

4.2.2 Low-Light Inspection Distance

To determine the appropriate inspection distance during varying low-light conditions - nautical and astronomical twilight, and night - to collect image data of defects on the Virginia Avenue bridge girder sample, the sUAS is flown at known distances from the web. The experiment seeks to determine what the effects of distance are during varying low-light conditions on the ability to capture images of defects on the

girder. The experiment was conducted at Purdue Universities S-BRITE facility under controlled conditions. The premise of experiment was to determine appropriate distances for the inspecting the steel girder for global damage using thermal imaging and RGB low-light camera in varying low-light conditions. The objectives of the experiment were:

- Determine the appropriate distance for capturing imagery of global damage during varying low-light conditions.
- Evaluate the difference if any in visually detecting damage and defects in steel girders during nautical and astronomical, and night conditions.
- Evaluate the capabilities of thermal imaging and RGB lowlight camera as an inspection tool for steel bridge inspection post-disaster.

Four low-light distance experiments were conduct on April 19, 2019 start at 9:29 pm during evening nautical twilight and ending at 10:12 pm at night. The temperature range for April 19, 2019 was 47 degrees Fahrenheit (8 Celsius) for the high and 40 degrees Fahrenheit (4 Celsius) for the low with a temperature differential of seven-degree Fahrenheit (4 Celsius) differential throughout the day. Air temperature at the time of the test was 43 degrees Fahrenheit (6 Celsius), four-degree (2 Celsius) differential from the daily high temperature, with a relative humidity of 80 percent. Winds were out of the north at 17 miles per hour.

The nautical twilight experiments began at 9:29 pm and was complete at 9:33pm. Evening nautical twilight for April 19, 2019 began at 9:00 pm and end at 9:34 pm. During astronomical twilight the experiments began at 9:43 pm and was complete at 9:54 pm. Evening astronomical twilight for April 19, 2019 began at 9:35 pm and end at 10:10

pm. The night experiments began at 10:11 pm and was complete at 10:13pm. Night for April 19, 2019 began at 10:11 pm and were completed at 10:13 pm.

The remote sensing platform for these experiments included the thermal imaging and RGB low-light camera mounted on the bottom of the six-rotor UAV with stabilizing 3-axis gimbal. The distance images were obtained by the sUAS from the Virginia Avenue Bridge's north bound steel girder began at four feet and then every two feet thereafter, out to 20 feet and flown perpendicular to the girder at approximately five feet (1.524m) AGL.

The following sections provide the results of each distance test, nautical twilight, astronomical twilight, and night.

4.2.2.1 Low-light Inspection Distance Imagery

None of the damage or defects were observed in the thermal images (Figure 15). This is most likely due to the low temperature range of the day and only 4-degree Fahrenheit (2 Celsius) difference from the day's high at the time of the experiment. Figure 9 shows the lack of detail visible in the thermal images, where even the five-inch (12.7 cm) diameter hole is not visible.

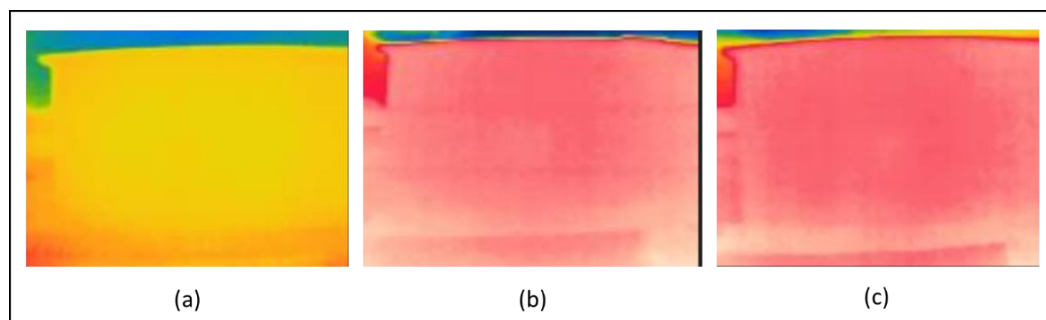


Figure 15: Thermal camera images of Virginia Ave girder from 6 ft: (a) Nautical twilight; (b) Astronomical Twilight; (c) Night.

The RGB low-light camera images at a distance of four feet (1.219m) all three cracks measuring 0.039 inches (1 mm) wide between mending plates one and two, 0.079 inches (2 mm) between mending plates two and three, and 0.138 inches (3.5 mm) below mending plate three were visible in the images captured by the RGB low-light camera during nautical and astronomical twilight, and night. Additionally, the five-inch (12.7 cm) diameter hole in the upper right of the images is visible along with rust on the web and marks from where the girder had been struck (Figure 16).

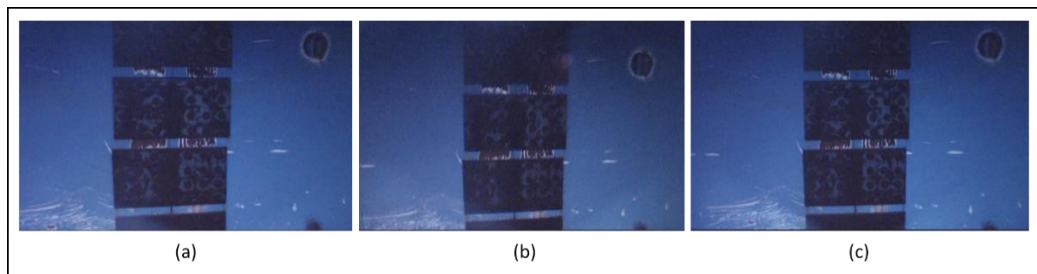


Figure 16: Low-Light RGB camera images of Virginia Ave girder from 4 ft: (a) Nautical twilight; (b) Astronomical Twilight; (c) Night.

At six feet (1.829m) from the web only the two larger cracks measuring 0.079 inches (2 mm) between mending plates two and three, and 0.138 inches (3.5 mm) below mending plate three were visible during nautical and astronomical twilight. During night the only crack visible in the image at six feet (1.829 m) is the crack measuring 0.138 inches (3.5 mm) below mending plate three. Again, the five-inch (12.7 cm) diameter hole in the upper right of the images are still visible along with rust between the mending plates and the lower right on the web, as well as the white marks in the blue paint coating on web where the girder had been struck (Figure 17).

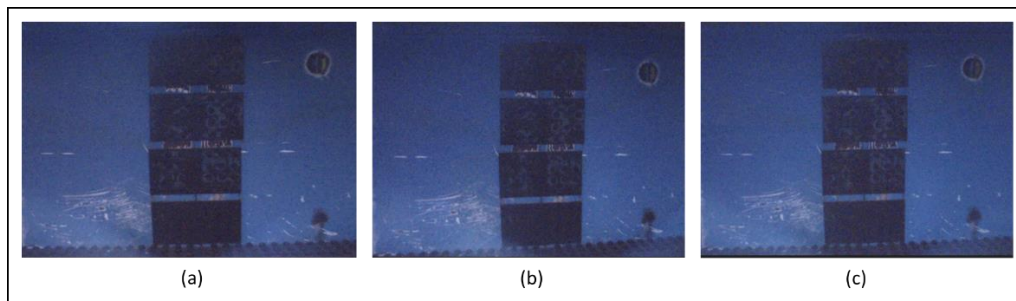


Figure 17: Low-Light RGB camera images of Virginia Ave girder from 6 ft: (a) Nautical twilight; (b) Astronomical Twilight; (c) Night.

At eight feet (2.438m) only the crack measuring .138 inches (3.5 mm) below mending plate three were visible in the images captured during nautical and astronomical, and night. Again, the five-inch (12.7 cm) diameter hole in the upper right of the images are still visible along with rust between the mending plates and the on lower right of the web, as well as the white marks in the blue paint coating from where the girder had been struck (Figure 18).

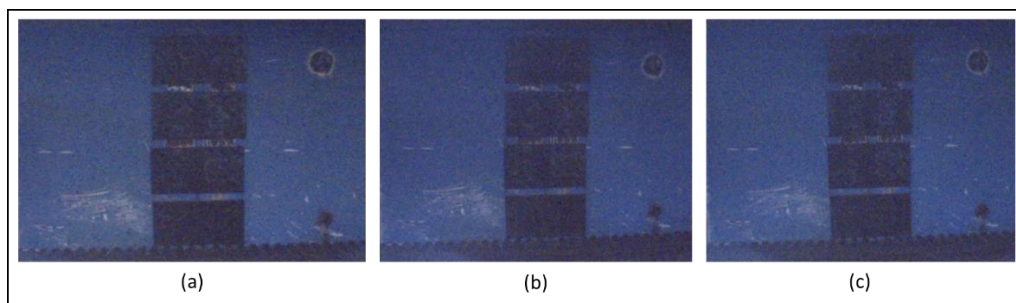


Figure 18: Low-Light RGB camera images of Virginia Ave girder from 8 ft: (a) Nautical twilight; (b) Astronomical Twilight; (c) Night.

At 10 feet (3.048m) none of the three cracks are visible, but the five-inch (12.7 cm) diameter hole in the upper right of the images are still visible although becoming less distinguishable for the rust on the web. The white marks in the blue paint coating on the web where the girder had been struck are still visible (Figure 19).

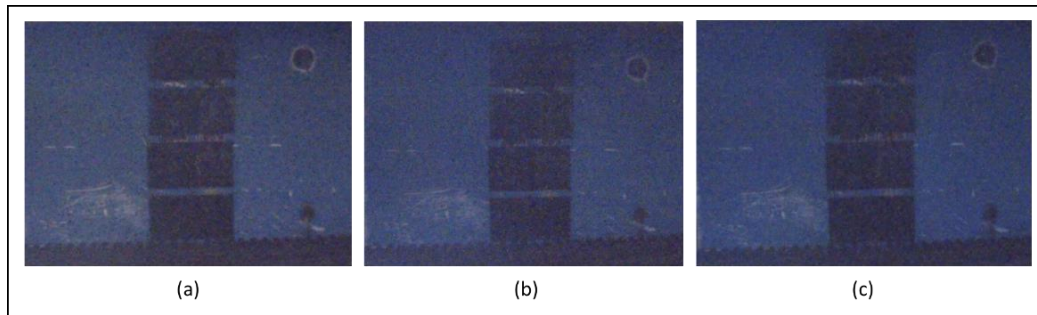


Figure 19: Low-Light RGB camera images of Virginia Ave girder from 10 ft: (a) Nautical twilight; (b) Astronomical Twilight; (c) Night.

At 12 feet (3.658m) none of the three cracks are visible and the five-inch (12.7 cm) diameter hole in the upper right of is distinguishable in the image captured during nautical twilight but is not distinguishable from the rust on the web in the astronomical twilight or night image. The rust between the mending plates is becoming less distinct on all three images but more so on the images captured during astronomical twilight and night. The white marks in the blue paint coating on the web from where the girder had been struck are still visible but are but are less apparent then from the ten-foot (3.048m) images (Figure 20).

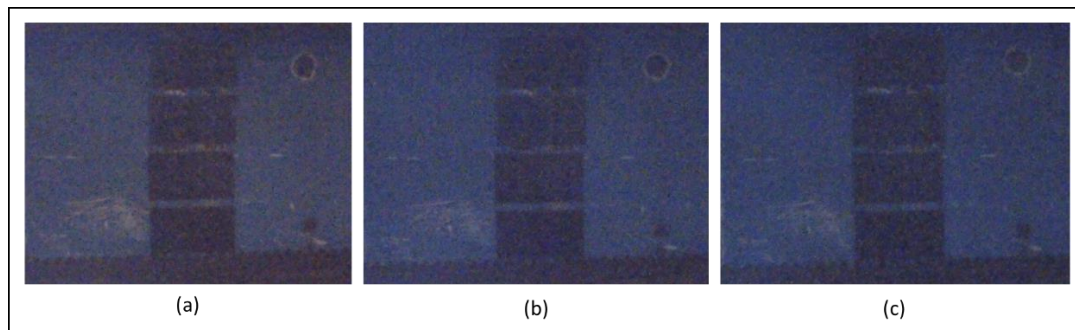


Figure 20: Low-Light RGB camera images of Virginia Ave girder from 12 ft: (a) Nautical twilight; (b) Astronomical Twilight; (c) Night.

At 14 feet (4.267m) none of the three cracks are visible and the five-inch (12.7 cm) diameter hole in the upper right of the images appears as rust. The rust between the mending plates has become less distinct between mending plates on the image captured during nautical twilight and difficult to identify as rust on the images captured during astronomical twilight and night. The white marks in the blue paint coating on the web where the girder had been struck are still visible but are less apparent on images captured during astronomical twilight and night (Figure 21).

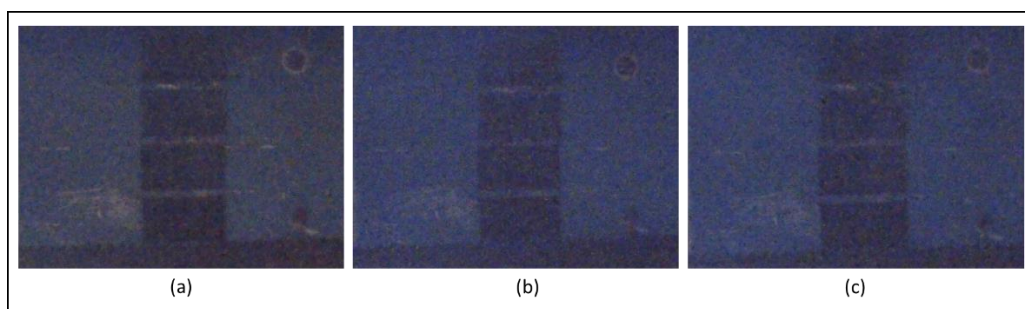


Figure 21: Low-Light RGB camera images of Virginia Ave girder from 14 ft: (a) Nautical twilight; (b) Astronomical Twilight; (c) Night.

At 16 feet (4.877m) none of the three cracks are visible and the five-inch (12.7 cm) diameter hole in the upper right of the images appears as rust in the images captured during nautical and astronomical twilight, and less so on the night image. The rust between the mending plates has become less distinct on the image captured during nautical twilight and difficult to identify as rust on the image captured during astronomical twilight, and indistinguishable on the image capture at night. The white marks in the blue paint coating on the web where the girder had been struck are slightly visible on the image captured at nautical twilight and even less distinct on images captured during astronomical twilight and night (Figure 22).

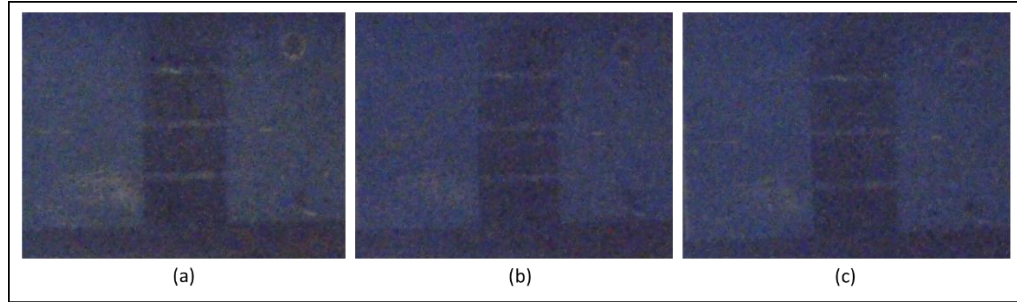


Figure 22: Low-Light RGB camera images of Virginia Ave girder from 16 ft: (a) Nautical twilight; (b) Astronomical Twilight; (c) Night.

At 18 feet (5.486m) none of the three cracks are visible and the five-inch (12.7 cm) diameter hole in the upper right of the images appears as rust in the image captured during nautical twilight and is less distinct in the image captured during astronomical twilight. The hole is no longer visible in the image captured during night. The rust between the mending plates has become less distinct on the image captured during nautical twilight and vaguely identifiable between mending plates two and three, and plates three and four on the image captured during astronomical twilight. The rust on the image captured during night is longer identifiable. The white marks in the blue paint coating on the web where the girder had been struck are less visible on the image captured at nautical twilight and difficult to identify on images captured during astronomical twilight and night (Figure 23).

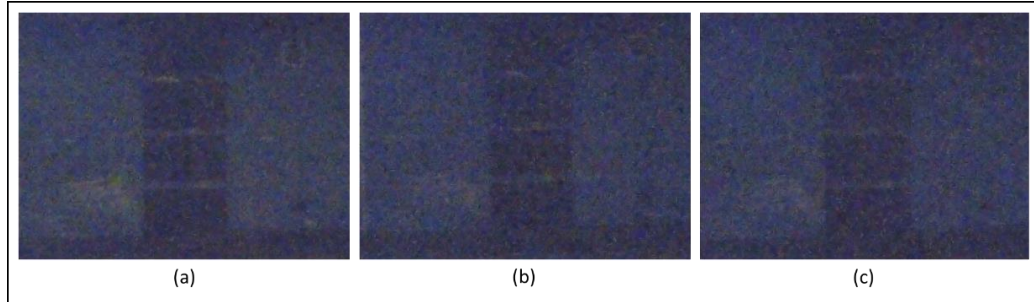


Figure 23: Low-Light RGB camera images of Virginia Ave girder from 18 ft: (a) Nautical twilight; (b) Astronomical Twilight; (c) Night.

At 20 feet (6.096m) none of the three cracks are visible and the five-inch (12.7 cm) diameter hole in the upper right of the images appears as rust in the images captured during nautical twilight and is not visible on the images captured during astronomical twilight and night images. The rust between the mending plates has become indistinguishable on all three images. The white marks in the blue paint coating on the web where the girder had been struck are vaguely visible on the images captured at nautical and astronomical twilight and not visible on image captured during night (Figure 24).

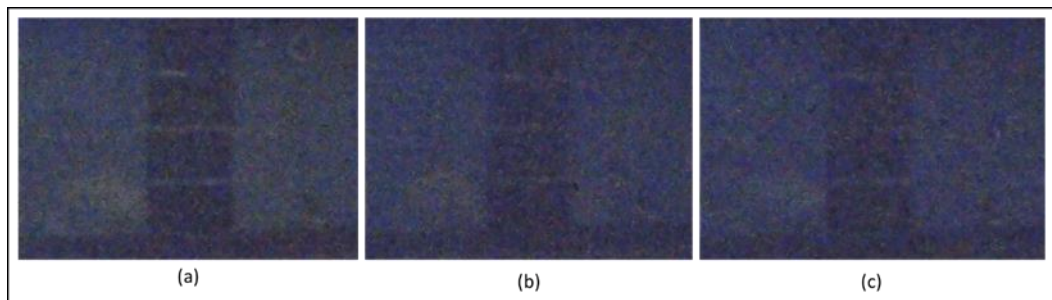


Figure 24: Low-Light RGB camera images of Virginia Ave girder from 20 ft: (a) Nautical twilight; (b) Astronomical Twilight; (c) Night.

Overall, as the distance increased as the sUAS flies further away, the resolution in the pictures became more granular making it difficult to see defects. This is expected since the higher ISO range of the image sensor in the camera - makes it more sensitive to light allowing the camera to capture images in low-light conditions – requires the platform to be stable (free of any movement) during the opening and closing of the aperture. Any slight movement will increase the granularity (noise) in the image. So, the higher the ISO the more granular the image can become.

4.2.2.3 Low-light Inspection Distance Tabular Data

Based off the section of the Virginia Ave steel girder used in the low-light inspection distance, four defects were recorded. The four defects were the crack in the web ranging from 0.039 inches (1 mm) to 0.138 inches (3.5 mm) in width, a hole in the web measuring five inches (12.7 cm) in diameter, impact scratches grouped into three areas on the web (white marks on right side, center, and left side of mending plates), and rust grouped into 6 areas on the web (Figure 25).

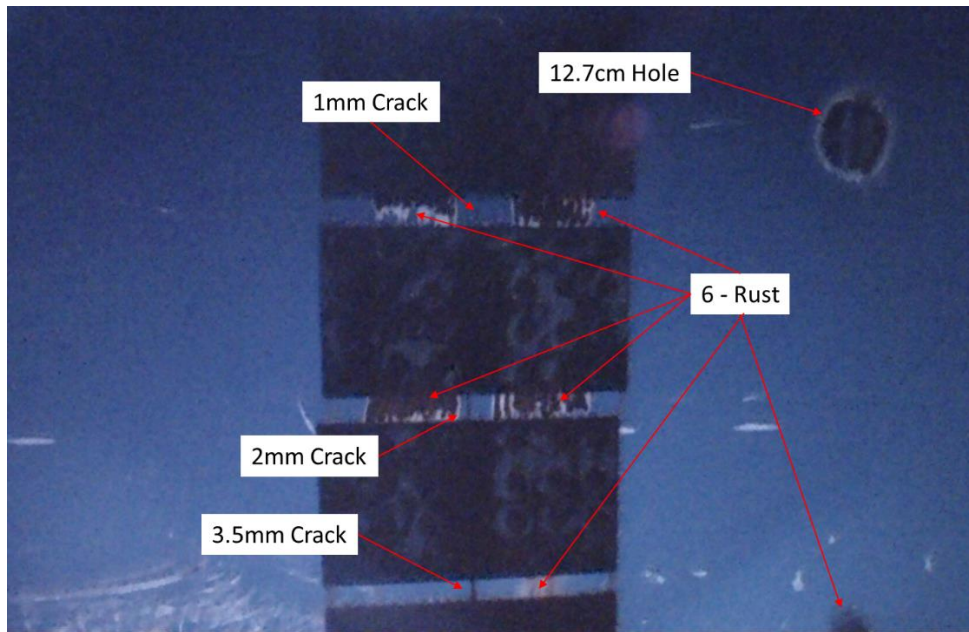


Figure 25: Damage and defects in Virginia Ave steel girder.

These four defect areas were used to score the imagery for statistical analysis. The data was organized by time of day based off the low-light conditions – nautical and astronomical twilight, and night. Figure 26 graphically represents the data of the effect time and distance on the ability to see defects in the imagery.

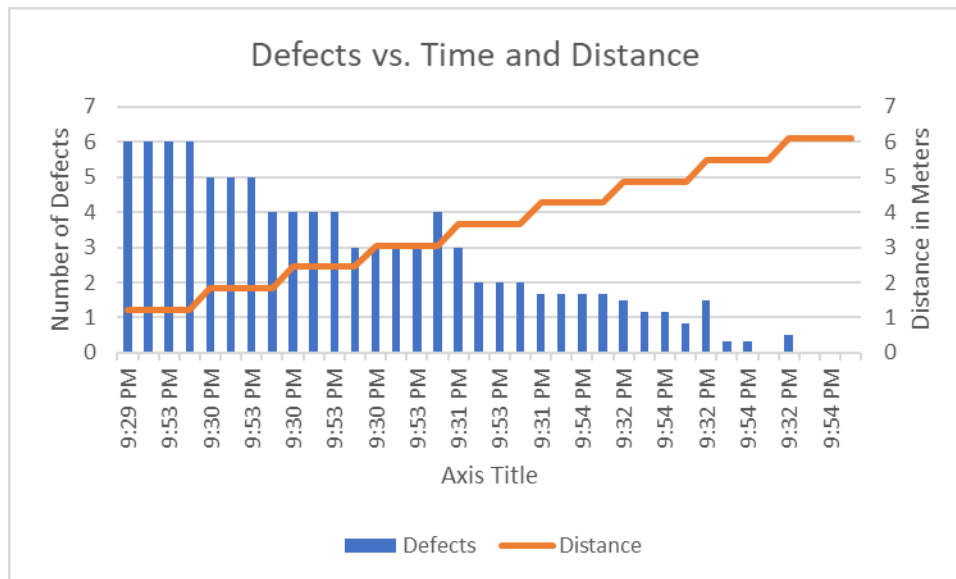


Figure 26: Defects versus time and distance.

Below are the tables for nautical and astronomical twilight, and night (tables 4, 5, 6, & 7). The cracks were scored with either 0 (not visible) or 1 (visible) for each size of crack. The hole was scored like the cracks but was score 0 for not being distinguishable from rust. The impact marks where divide into three groupings. They were scored either three of three, two of three, one of three, or zero of three based on ability to distinguish the marks in the imagery. The rust was divided into six groupings and scored from six of six thru zero of six based on the ability to distinguish the rust groupings in the imagery.

Table 4: Defects recorded for each time interval at known distance

Distance 1.22m		Distance 1.83m		Distance 2.44m		Distance 3.04m	
Time	Defects	Time	Defects	Time	Defects	Time	Defects
9:29 PM	6	9:30 PM	5	9:30 PM	4	9:30 PM	3
9:42 PM	6	9:42 PM	5	9:42 PM	4	9:42 PM	3
9:53 PM	6	9:53 PM	5	9:53 PM	4	9:53 PM	3
10:12 PM	6	10:12 PM	4	10:12 PM	3	10:12 PM	4

Distance 3.66m		Distance 4.27m		Distance 4.88m		Distance 5.49m	
Time	Defects	Time	Defects	Time	Defects	Time	Defects
9:31 PM	3	9:31 PM	1.67	9:32 PM	1.5	9:32 PM	1.5
9:43 PM	2	9:43 PM	1.67	9:43 PM	1.17	9:43 PM	0.33
9:53 PM	2	9:54 PM	1.67	9:54 PM	1.17	9:54 PM	0.33
10:12 PM	2	10:12 PM	1.67	10:12 PM	0.83	10:12 PM	0

Distance 6.1m	
Time	Defects
9:32 PM	0.5
9:43 PM	0
9:54 PM	0
10:13 PM	0

Table 5: Defects observed during nautical twilight at known distances

Distance (m)	Crack Width			Hole	Impact	Rust	Overall Defects
	1 mm	2 mm	3.5 mm	12.7 cm	Scratches		
1.22	1	1	1	1	1	1	6
1.83	0	1	1	1	1	1	5
2.44	0	0	1	1	1	1	4
3.05	0	0	0	1	1	1	3
3.66	0	0	0	1	1	1	3
4.27	0	0	0	0	1	0.67	1.67
4.88	0	0	0	0	1	0.50	1.50
5.49	0	0	0	0	1	0.50	1.5
6.1	0	0	0	0	0.33	0.17	0.50

Table 6: Defects observed during astronomical twilight at known distances
Astronomical Twilight

Distance (m)	Crack Width			Hole	Impact	Rust	Overall Defects
	1 mm	2 mm	3.5 mm	12.7 cm	scratches		
1.22	1	1	1	1	1	1	6
1.83	0	1	1	1	1	1	5
2.44	0	0	1	1	1	1	4
3.05	0	0	0	1	1	1	3
3.66	0	0	0	0	1	1	2
4.27	0	0	0	0	1	0.67	1.67
4.88	0	0	0	0	0.67	0.5	1.17
5.49	0	0	0	0	0.33	0	0.33
6.1	0	0	0	0	0	0	0

Table 7: Defects observed during night at known distances

Distance (m)	Crack Width			Hole	Impact	Rust	Overall Defects
	1 mm	2 mm	3.5 mm	12.7 cm	scratches		
1.22	1	1	1	1	1	1	6
1.83	0	0	1	1	1	1	4
2.44	0	0	0	1	1	1	3
3.05	0	0	1	1	1	1	4
3.66	0	0	0	0	1	1	2
4.27	0	0	0	0	1	0.67	1.67
4.88	0	0	0	0	0.33	0.50	0.83
5.49	0	0	0	0	0	0	0
6.1	0	0	0	0	0	0	0

The data from these tables was used for regression analysis to examine the relationship between time of day and distance effect on the imagery of defects using the RGB low-light camera systems.

4.2.3 Validation Test

The validation test flights were flown on May 15th, 2019 at the S-BRITE center. Nautical twilight was from 9:29pm thru 10:07pm, astronomical twilight was from 10:08pm thru 10:50pm, and night began at 10:51pm. The Virginia Ave bridge girder was used for the validation test. The temperature range for the day was 74 degrees Fahrenheit (23 Celsius) and 47 degrees Fahrenheit (8 Celsius) and during the test was 59 degrees Fahrenheit (15 degrees Celsius) a difference of 15 degrees Fahrenheit (8 Celsius). Humidity was 84 percent and the winds were calm. Three flights were flown, one during nautical twilight at 9:46 pm, one during astronomical twilight 10:08 pm, and one during night at 10:52 pm. The west side of the steel girder was used for the validation. The sUAS was piloted in angle flight mode during all three flights.

To validate the results of the low-light distance experiment, three cones were placed seven feet (2.13m) from the Virginia Ave steel girder running parallel to the girder. These cones served as known distances points for the pilot to fly and capture imagery of the steel girder web. The altitude of the sUAS was approximately 5 feet 7 inches (1.73m) AGL, the same altitude as the low-light distance experiment.

The first flight at nautical twilight, the 0.079 inches (2 mm) and 0.138 inches (3.5 mm) crack in the web, the five-inch (12.7 cm) hole, rust, and impact scratches on the south end of the girder were visible in the RGB lowlight images (Figure 27a). Thermal image confirmed the presences of the five-inch (12.7 cm) hole but the cracks and rust were not confirmed in the thermal image (Figure 27b). The cracks were not visible in the thermal image. The one-inch (2.54cm) diameter holes and three-inch diameter hole (7.62cm) on the north end of the steel girder were visible (Figure 28a) but the 0.1 mm

crack was not visible. The thermal image validated the one-inch (2.54cm) diameter holes (Figure 28b) and the three-inch (7.62cm) diameter hole.

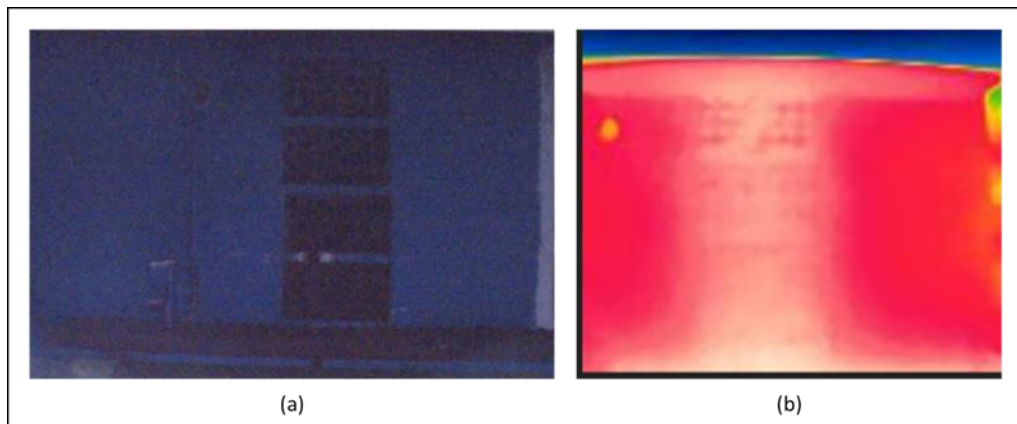


Figure 27: Low-Light RGB (a) and thermal (b) camera images of southwest side of the Virginia Ave girder during nautical twilight from 8 ft.

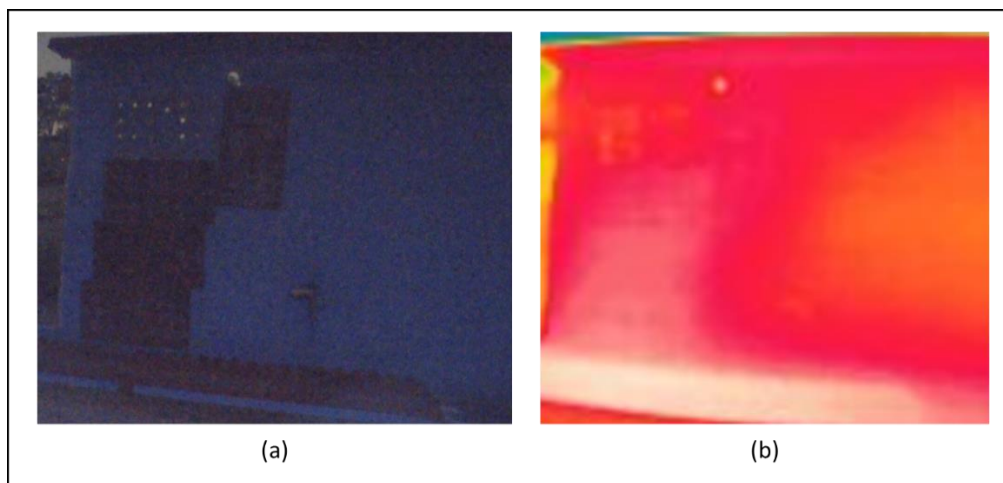


Figure 28: Low-Light RGB (a) and thermal (b) camera images of northwest side of Virginia Ave girder during nautical twilight from 8 ft

The second flight was at astronomical twilight and the 0.039 inches (1 mm) crack in the web was visible but the 0.079 inches (2 mm) and 0.138 inches (3.5 mm) crack were not. Additionally, the five-inch (12.7 cm) hole, rust, and impact scratches on the south

end of the girder were visible in the RGB lowlight images (Figure 29a). Thermal image confirmed the presences of the five-inch (12.7 cm) hole but the cracks and rust were not confirmed in the thermal image (Figure 29b). The one-inch (2.54 cm) diameter holes and three-inch diameter hole (7.62 cm) on the north end of the steel girder were visible (Figure 30a) but the 0.1 mm crack was not visible. The thermal image validated the one-inch (2.54 cm) diameter holes and the three-inch (7.62 cm) diameter hole (Figure 30b).

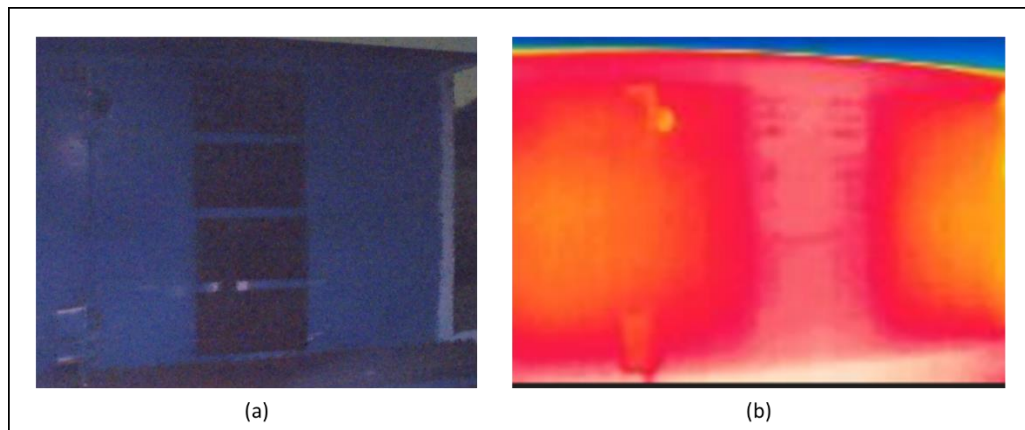


Figure 29: Low-Light RGB (a) and thermal (b) camera images of southwest side of Virginia Ave girder during astronomical twilight from 8 ft (2.44m).

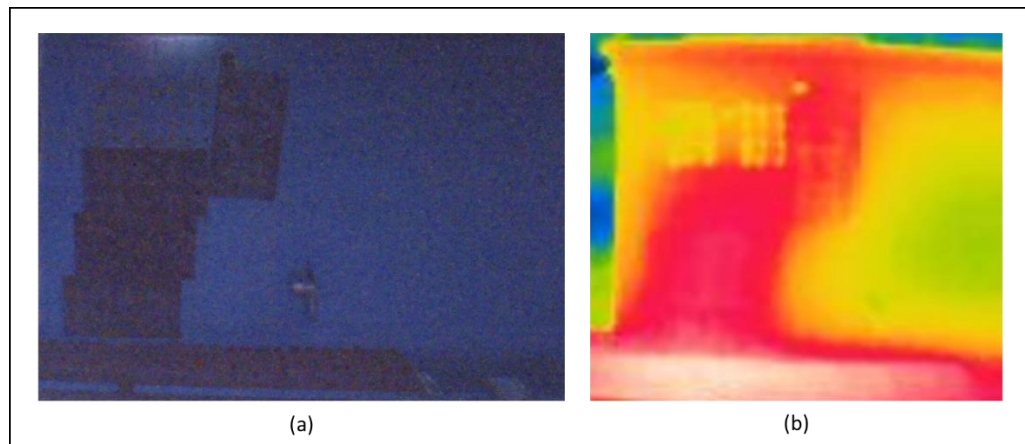


Figure 30: Low-Light RGB (a) and thermal (b) camera images of northwest side of Virginia Ave girder during astronomical twilight from 8 ft (2.44m).

The third flight was at night and the 0.138 inches (3.5 mm) crack in the web was visible but the 0.039 inches (1 mm) and 0.079 inches (2 mm) crack were not. Additionally, the five-inch (12.7 cm) hole, rust, and impact scratches on the south end of the girder were visible in the RGB lowlight images (figure 31a). Thermal image confirmed the presences of the five-inch (12.7 cm) hole but the cracks and rust were not confirmed in the thermal image (Figure 31b). The one-inch (2.54 cm) diameter holes and three-inch diameter hole (7.62 cm) on the north end of the steel girder were visible (Figure 32a) but the 0.1 mm crack was not visible. The thermal image validated the one-inch (2.54cm) diameter holes and the three-inch (7.62cm) diameter hole (Figure 32b).

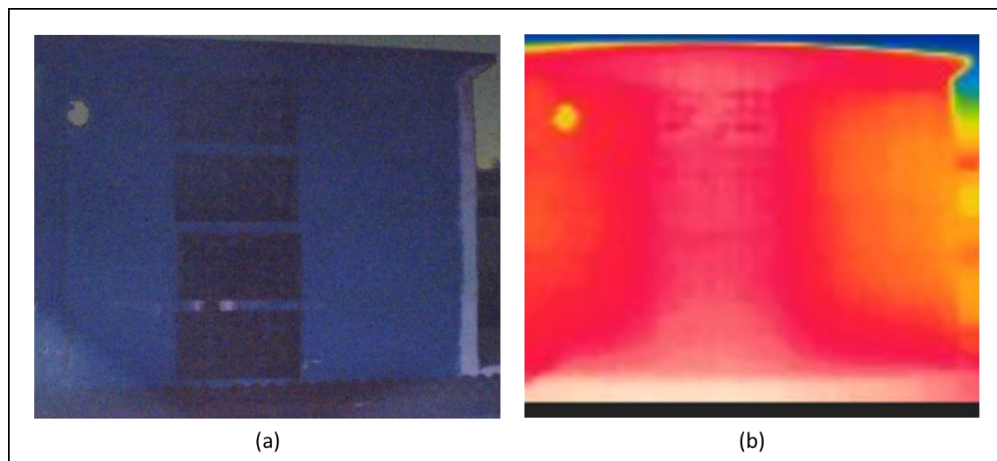


Figure 31: Low-Light RGB (a) and thermal (b) camera images of southwest side of Virginia Ave girder during night from 8 ft (2.44m).

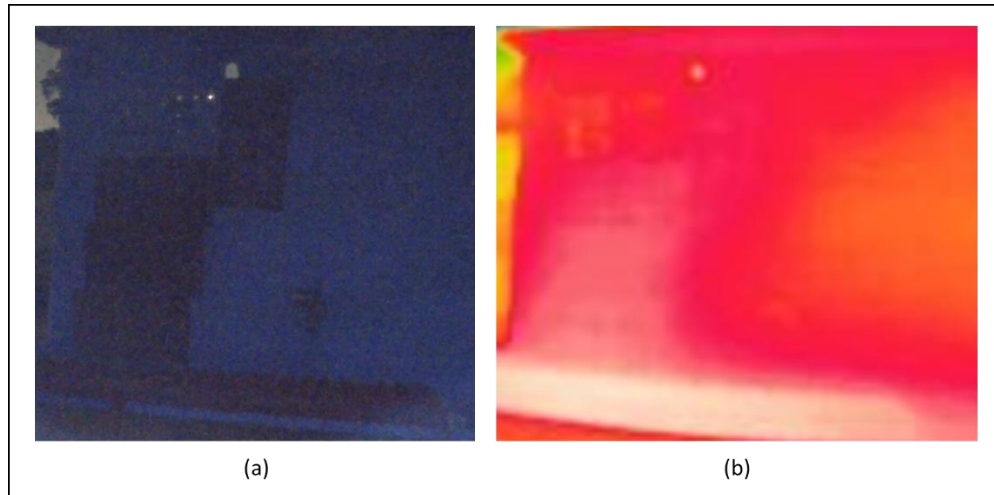


Figure 32: Low-Light RGB (a) and thermal (b) camera images of northwest side of Virginia Ave girder during night from 8 ft (2.44m).

Table 8 shows the defects observed from the sUAS imagery during the validation test. The data shows at seven feet (2.13m) the sUAS imagery could provide enough detail to observe global damage and defects in the steel girder.

Table 8: Validation data of defect observed at seven feet (2.13m)

Todd	Validation Flight (2.13m)							Overall Defects
	Crack Width			Hole	Holes	Impact	Rust	
	1 mm	2 mm	3 mm	(12.7cm)	(2.45cm)	scratches		
Nautical	0	1	1	1	1	1	1	6
Astronomical	1	0	0	1	1	1	1	5
Night	0	0	1	1	1	1	1	5

4.3 Analysis

In this section the data analysis for the three research questions is presented.

4.3.1 Research Question One Data

1. What is the effect of low-light conditions on the sUAS optics to assess global structural damage?

The initial field tests on the two steel girder bridge members demonstrate the sUAS capability to detect global damage to steel girders – a critical member of steel bridge superstructure - in low visibility condition. Of all the thermal imaging color pallets, rainbow and white hot had the best image quality of the damage and thus were selected for the initial test. Based on the images presented in section 4.2.1, the thermal color pallet rainbow was determined to be better than white hot for detecting damage on steel girders. The multiple colors of the rainbow pallet allowed for more temperature differentiation which assists in detecting cracks in the steel girders.

The RGB low-light images captured details of the defects in both steel girder samples. These images provided enough details to detect the cracks, hole, impact marks, and rust on the girder samples.

Regression analysis of damage and defects versus time test was conducted using the data from tables 5, 6, and 7 with an alpha of .05 for 95% confidence level with the following hypothesis test:

H_0 : There is no relationship between low-light conditions (nautical and astronomical twilight, and night) and observing defects in the imagery of the sUAS.

H_a : There is a relationship between low-light conditions (nautical and astronomical twilight, and night) and observing defects in the imagery of the sUAS.

Table 9 provide the analysis of variance test for defects versus time. The resulting p -value for time of day from the test was 0.482. Therefore, the null hypothesis is not rejected, thus with 95% confidence there is insufficient evidence to conclude there is a relationship between low-light conditions and observing defects in images.

Table 9: Analysis of variance of defect versus time.

Source	DF	Adj SS	Adj MS	F-Value	P-Value
Regression	1	1.907	1.907	0.51	0.482
Time	1	1.907	1.907	0.51	0.482
Error	34	128.147	3.769		
Lack-of-Fit	8	78.224	9.778	5.09	0.001
Pure Error	26	49.923	1.920		
Total	35	130.053			

Table 10 provides the model summary of defects versus time of day. The r -squared shows 1.47% of the variance in the model is explained by time of day and the r -squared adjusted and r -squared predicted are 0.00%. This further supports the null hypothesis time of day is insufficient in observing defects in the steel girder.

Table 10: Defects versus time model summary.

S	R-sq	R-sq(adj)	R-sq(pred)
1.94140	1.47%	0.00%	0.00%

4.3.2 Research Question Two Data

1. What effect does distance have on the sUAS camera imagery in observing damage and defects in the structural steel during low-light conditions?

To determine the effects of distance on the imagery taken from the sUAS camera during low-light conditions, regression analysis of defects versus distance was conducted

using the data from table 4, an alpha of .05 for 95% confidence level and the following hypothesis test:

H₀: There is no relationship between distance during low-light conditions (nautical and astronomical twilight, and night) and observing defects in the imagery of the sUAS.

H_a: There is a relationship between distance during low-light conditions (nautical and astronomical twilight, and night) and observing defects in the imagery of the sUAS.

Table 11 provides the analysis of variance for defects versus distance. The f-value is relatively high and is identical for the model and intercept. The resulting *p*-value for the model and distance from the test was 0.000. Therefore, the null hypothesis is rejected, thus with 95% confidence there is sufficient evidence to conclude there is a relationship between distance and observing defects in images during low-light conditions. The f-value for the lack of fit is not statistically significant with a *p*-value of 0.058 but is only 0.008 from being significant. This is important because lack of fit indicates possible missing predictors.

Table 11: Analysis of variance defects versus distance.

Source	DF	Adj SS	Adj MS	F-Value	P-Value
Regression	1	122.551	122.551	555.39	0.000
Distance	1	122.551	122.551	555.39	0.000
Error	34	7.502	0.221		
Lack-of-Fit	7	2.789	0.398	2.28	0.058
Pure Error	27	4.713	0.175		
Total	35	130.053			

Table 12 provides the model summary of defects versus distance. The r-squared shows 94.23% of the variance in the model is explained by the distance for the steel girder with the r-squared adjusted at 94.06% and r-squared predicted 93.48% show sufficient evidence distance is a reliable predictor in observing defects in the steel girder.

Table 12: Model Summary of defects versus distance.

S	R-sq	R-sq(adj)	R-sq(pred)
0.469743	94.23%	94.06%	93.48%

The regression equation for the defects versus distance in figure 33 state for every 2 feet (0.61 m) increase in distance the sUAS is from the steel girder the number of damage and defects visible in the imagery is reduced by 1.1714.

$$\text{Defects} = 6.899 - 1.1714 \text{ Distance}$$

Figure 33: Regression equation for defects versus distance.

Table 13 provides the analysis of variance for defects versus distance and low-light conditions, using a p -value of .05 for 95% confidence level. The resulting p -value for both low-light conditions at 0.029 and distance at 0.000 were both statistically significant as was the model at 0.000. Additionally, table 14 shows the r-squared at

95.02% indicates the model accounts for a majority of the variance and r-squared predicted at 93.88% show the model is a reliable predictor for observing defects in the imagery for new observations.

Table 13: Analysis of variance of defects versus time and distance.

Source	DF	Adj SS	Adj MS	F-Value	P-Value
Regression	2	123.579	61.789	314.92	0.000
Time	1	1.028	1.028	5.24	0.029
Distance	1	121.672	121.672	620.12	0.000
Error	33	6.475	0.196		
Total	35	130.053			

Table 14: Model Summary of Defects versus time and distance.

S	R-sq	R-sq(adj)	R-sq(pred)
0.442952	95.02%	94.72%	93.88%

Table 15 provides the regression coefficients of defects versus time and distance. Both time at -15.99 and distance at -1.1679 coefficients are negative. For time this indicates that as evening hours progress from nautical twilight into astronomical twilight and into night the less defects are observable in the imagery. For distance this indicates as the distances increases the less defects are observable in the imagery.

Table 15: Coefficients of Defects versus time and distance.

Term	Coef	SE Coef	T-Value	P-Value	VIF
Constant	21.43	6.35	3.37	0.002	
Time	-15.99	6.99	-2.29	0.029	1.00
Distance	-1.1679	0.0469	-24.90	0.000	1.00

The regression equation for the defects versus time and distance in figure 13 states for every 2 feet (0.61 m) increase in distance the sUAS is from the steel girder the number of damage and defects visible in the imagery is reduced by 1.1714.

$$\text{Defects} = 21.43 - 15.99 \text{ Time} - 1.1679 \text{ Distance}$$

Figure 34: Regression equation for defects versus time and distance.

4.3.3 Research Question Three Data

3. What is the logical correlation, if any, between the sUAS cameras imagery to observe damage and defects during low-light conditions at a given distance?

To determine whether there is a correlation between the sUAS cameras imagery to observe defects, and low-light conditions, a Pearson correlation test was performed on defects, distance, and time using the data from tables 5, 6, and 7 with an alpha of .05 for 95% confidence level and the following hypothesis test:

H_0 : There is no correlation between observing defects in the imagery, distance from the steel girder, and the low-light conditions (nautical and astronomical twilight, and night).

H_a : There is no correlation between observing defects in the imagery, distance from the steel girder, and the low-light conditions (nautical and astronomical twilight, and night).

Table 16. provides the values of the Pearson correlation test. The results show there is a strong negative correlation, -0.971, with a p -value of 0.000, between observing defects in the imagery and the distance the sUAS camera is from the steel girder. This provides sufficient evidence there is a strong negative correlation between the distance the sUAS is from the steel girder and observing defects in the imagery. There is a weak negative correlation, -0.121 with a p -value of 0.121, between observing defects in the imagery and low-light conditions. This provides insufficient evidence of a correlation

between defects observed in the imagery and low-light conditions. Therefore, the null hypothesis is rejected, thus with 95% confidence there is sufficient evidence to conclude there is a correlation between distance and observing defects in images during low-light conditions.

Table 16: Pearson Correlation for defects, time, and distance.

	Time	Defects
Defects	-0.121	0.482
Distance	0.033	-0.971
	0.848	0.000

4.4 Summary

This chapter provided the visual and statistical analysis of the three experiments, as well as analysis and results of the three research questions. The results from the imagery captured by sUAS equipped with an RGB low-light and thermal camera showed the system was capable of detecting damage and defects down to 0.039 inches (1 mm) in steel girders. Images from the thermal imaging camera had mixed results with some imagery showing evidence of detecting 0.138 inches (3.5 mm) crack in the steel girder. The results and analysis showed the sUAS provides an additional tool for recovery managers to inspect for structural damage and defects to steel girders during low-light conditions, by allowing inspection operations for global damage 24 hours a day. The next chapter will discuss the major finding from the analysis and results, provide recommendations and future research.

CHAPTER 5. DISCUSSION

This chapter discusses the results of the experiments and the data analysis of presented in Chapter 4 which tested the RGB low-light and thermal imaging camera ability to capture images of damage and defects in the steel girder as well as the research questions:

1. What is the effect of low-light conditions on the sUAS optics to assess global structural damage?
2. What effect does distance have on the sUAS camera imagery in observing damage and defects in the structural steel during low-light conditions?
3. What is the logical correlation, if any, between the sUAS camera imagery to observe damage and defects during low-light conditions at a given distance?

The chapter discusses the major finding from the data analysis, contributions to knowledge, make recommendations, and potential future research.

5.1 Major Findings

This section will discuss the major findings from the data analysis in Chapter 4.

5.1.1 Preliminary Field Test

The preliminary field test findings established the ability to observe damage and defects from the imagery obtained by RGB low-light and thermal camera. The RGB low-light images provide excellent details of the damage and defects on both the NSR railroad girder and the Virginia avenue Bridge girder. All three cracks; 0.039 inches (1 mm), 0.079 inches (2 mm), and 0.138 inches (3.5 mm), were visible in the RGB low-light image of the Virginia Avenue Bridge from a horizontal distance of 4 feet (1.22 m)

perpendicular to the web. Additionally, the RGB low-light image of the NSR railroad girder provide excellent details showing the 0.748 inches (19 mm) hole and rust flakes resting on the bottom flange of the girder.

Although the thermal images lack details of the RGB low-light image, the thermal image of the NSR railroad girder confirmed the 0.748 inches (19 mm) hole and the rust flakes resting on the bottom flange. The experiment also determined the rainbow color pallet as the best for observing damage and defects in the steel girders. Although details of each crack in the Virginia Avenue bridge girder thermal images where not observable, the 0.138 inches (3.5 mm) crack in the rainbow pallet as well as the area of the mending plates was discernable.

5.1.2 Low-Light Inspection Distance Findings

In analyzing the effects of distance on the sUAS camera during low-light conditions, images captured during nautical and astronomical twilight, and night were taken at known distances. The analysis of variance of defects versus time and distance, both time and distance were statistically significant with an $\alpha = .05$. The R-squared in the model defects versus time and distance was 95.02% accounting for a majority of the variance and the R-squared predictive at 93.88% show strong evidence the model would predict the observation of damage and defects in steel girders. While time and distance were statistically significant in the model, the Pearson's correlation indicated a strong negative correlation between defects and distance, and a weak negative correlation between defects and time. This means there is evidence of a strong relationship between the distance from the steel girder and the ability to detect damage and defects from the imagery.

When regression analysis conducted on defects versus time the results showed time as a predictor of damage and defects observed in the imagery was not statically significant with an $\alpha = .05$. Furthermore, the R-squared was 1.47% accounting for very little of the variance in observation of damage and defects in the imagery. On the contrary, conducting regression analysis of defects versus distance the results showed distance as a predictor of observing damage and defects in the imagery was statistically significant with a an $\alpha = .05$. The R-squared for defects versus distances was 94.23% accounting for the majority of variance in the model. The R-squared predictive at 93.48% further supports evidence that distance is a better predictor of observing damage and defects in imagery captured by the sUAS in low-light conditions. With only a 0.4% difference in the variance accounted for between defects versus distance and defects versus time and distance, time is not seen as a significant predictor in the model.

5.1.3 Validation Findings

The validation experiment confirmed the suitable distance range for the sUAS for observing damage and defects was 4 feet (1.22 m) to 8 feet (2.44 m). Furthermore, the experiment affirmed that distance is the primary factor in observing damage and defects, as they were observed in all imagery captured during nautical and astronomical twilight, and night.

In addition to the thermal imagery captured during the validation experiment provide confirmation of the five-inch (12.7 cm) hole and the one-inch (2.54 cm) holes. The temperature differential between the high at 74 degrees Fahrenheit (23 Celsius) and the time of the experiment 59 degrees Fahrenheit (15 Celsius) was a differential of 15 degrees Fahrenheit (8 Celsius). The higher temperature throughout the day allow the steel

girder to absorb more heat thus providing a better temperature differential between the damaged and defected areas and the painted areas of the steel girder.

5.2 Discussion

5.2.1 Preliminary Field Test

Although, the thermal images were not as clear as the RGB lowlight camera image, two images can be overlaid on the ground control station's screen allowing for further details to be analyzed. Also, it is important to note when the images are overlaid on the ground control station, providing real-time images of the RGB low-light and thermal images for further visual analysis, the opacity of the thermal image can be adjusted.

The dual capability of the camera can help confirm areas that may appear as rust but are a hole in the girder. The thermal image colors assigned to the different temperatures would show a hole cooler than an area with rust which appears hotter. Additionally, the experiment affirmed Otero *et al.* (2015) finding that “maneuverability testing results showed that the sUAS could be properly operated by a skilled operator at a minimum clearance of 3 feet (0.91 m) from a target and with constant wind speeds of 15mph”, in this case 4 feet (1.22 m) and during low-light conditions with a wind speed of 17mph.

The preliminary field experiment provides proof of concept the sUAS imagery provided enough detail to observe damage in a steel girder down to 0.039 inches (1 mm) during low-light conditions. The dual images captured by the camera showed the value of the both images as the thermal image was able to validate the 0.138 inches (3.5 mm) in the Virginia Avenue bridge girder.

5.2.2 Low-Light Inspection Distance

The low-light inspection distance experiment established the suitable distance range was between four feet (1.22 m) and eight feet (2.44 m) to observe global damage in the steel girder. At eight feet (2.44 m) the 0.138 inches (3.5 mm) crack was still visible in the imagery during nautical and astronomical twilight. While the crack was not visible at eight feet (2.44 m) during night hours it was visible at 10 feet (3.05 m) during night hours. This anomaly could have been due to the stability of the sUAS when the image was captured. Due to this anomaly during night hours the distance of the cones for the validation test was seven feet (2.13 m) for the validation test.

The p-value of 0.000 in the regression analysis and coefficients showed distance as a significant factor in observing damage and defects during low-light conditions. This analysis further supported the distance range between four feet (1.22 m) and eight feet (2.44 m) with the coefficient for distance -1.1679.

Although the thermal images did not confirm any of the damage and defects in the steel girder, this may have been caused by the low temperatures and temperature differentiation of 4 degrees Fahrenheit from the daily high of 47 degrees Fahrenheit. Throughout the entire day, temperature differential was only seven-degree Fahrenheit and temperature differential from the daily low was only 3 degrees at the time of the experiment. The four-degree Fahrenheit differential between the daily high of 47 degrees Fahrenheit and 43 degrees Fahrenheit at the time of the experiment may have contributed to lack of detail based on the thermal properties of the steel girder and the low air temperatures throughout the day. This may prove to be an issue in areas involving low visibility conditions where smoke, fog, and dust impede the RGB lowlight camera.

5.2.3 Validate Experiment

The validation experiment confirmed the results of the distance range from the low-light inspection distance experiment. All three flight, one each during nautical and astronomical twilight, and night, at seven feet (2.13 m) from the steel girder the global damage and defects were observed in the sUAS imagery. This establishes a distance range for the imagery obtained from the sUAS to observe global damage in steel girders.

Additionally, the thermal images obtained during the validation test supports the higher daily temperatures and temperature differential throughout the day, 27-degree Fahrenheit, in aiding the observation of global damage in the steel girder. The temperature differential for the initial field test, 20 degrees Fahrenheit, was simpler to the validation test, adding to the higher temperature differential aiding in the thermal picture. The thermal images were capable of observing one-inch (2.54 cm) holes in the steel girder during the validation flights. Having the dual capability of the RGB low-light and thermal imaging camera confirms area on the steel girder that may be dismissed as rust as the thermal imaging show the temperature difference through color differences in the rainbow pallet.

5.3 Conclusion

A visual based approach for detecting damage and defects on steel girder during low-light conditions was proposed using imagery from sUAS. The steel girder images were obtained using a sUAS equipped with RGB low-light and thermal imaging camera. The preliminary field experiment showed proof the imagery from RGB low-light camera could detect 0.039 inches (1 mm) crack, 0.748 inches (19 mm) hole, impact marks, and rust on the steel girder during nautical twilight. Additionally, the experiment showed the

thermal imagery was capable of detecting 0.138 inches (3.5 mm) crack and rust flakes on the steel girder.

The low-light distance experiment established a suitable distance range for detecting the damage and defects in the steel girder between four feet (1.22 m) and eight feet (2.44 m). The experiment showed consistent results during nautical and astronomical twilight, and night. The data obtained from the imagery showed distance as the primary factor in detecting damage during low-light conditions. Additionally, distance account for 93.48% of the variance in the model, leaving only 6.52% of the variance accounted for by other variables. The validation experiment further showed the sUAS camera was highly effective at detecting damage and defects in the steel girder. All three flights during nautical and astronomical twilight, and night yield positive results in detecting the 0.138 inches (3.5 mm) crack and one-inch (25.4 mm) holes in the steel girder.

The necessity of ascertaining the condition of bridges – critical components of transportation infrastructure – motivates investigation for use of UAV-RS in low visibility conditions to assess damages to bridge critical components. Critical components of bridges with steel superstructure include: Rolled steel Multi-Beam and Fabricated Steel Multi-Girders; Steel Two-Girder Systems; Steel Pin-and-Hanger assemblies; Gusset plates; Steel Eye-bars; and Bridge Bearings (Ryan *et al.*, 2012). Inspecting these critical components using UAV-RS post disaster in lowlight conditions to assess bridge critical load bearing members for global damage, which is damage with a high probability of bridge failure when live loads are added.

With 9.1 percent of bridges in the United States deemed structurally deficient (ASCE, 2017), the ability to conduct rapid assessments of bridges following a disaster

event is essential for response and recovery operations to safely traverse routes. Barfuss *et al.* (2012) noted “the fact that aerial images can be collected and viewed within a matter of a few hours is extremely valuable to many UDOT applications such as road construction and road damage”. The utilization of UAV-RS during lowlight provides for “around the clock” assessments to identify viable primary and secondary routes into and out of areas requiring access. Furthermore the experiment showed the sUAS can provide information pertaining to the status of structural steel members following a disaster event as Lovelace (2015) and Wells *et al.* (2017) noted, UAVs imagery can be used for pre-planning for larger scale inspections by providing important details from a pre-inspection flight. Furthermore, the use of sUAS following a disaster event can improve the logistics by identifying the needs more actually based of the imagery collected. Lovelace (2015) found sUAS alleviate the logistical challenges of inspecting structures in difficult to reach locations by providing an efficient and effective way to inspect the structures. The results from this research showed the difficulties associated with low-light conditions can be alleviated as well.

Although there are still challenges noted in several studies using sUAS - FAA requirements, flight in GPS denied areas, data processing time, and acceptance of data by bridge owners (Barfuss *et al.*, 2012; Brooks *et al.*, 2015; Dorafshan *et al.*, 2017; Melo *et al.*, 2017; Wells & Lovelace, 2017) - the analysis from the data provided by the imagery obtained from the sUAS has several interesting results. The results showed the sUAS is a viable tool to inspect structure steel for damage and defects in low-low light conditions. This capability enable recovery manages the capability to conduct around the clock assessments of infrastructure. In addition to emergency inspections, the UAV-RS can be

used for search and rescue operations, making the UAV-RS a multipurpose enabler to practitioners in emergency management.

Reliable bridge assessments following a disaster reduces the risk of catastrophic failure, compounding an already difficult recovery effort with possibilities of more casualties. The visual information provided by UAV-RS during lowlight condition enables recovery managers to plan primary and alternate routes for response personal and those attempting to evacuate in a timelier manner.

5.4 Recommendations

As thermal images of bridge decks are an accepted way to inspect for concrete delamination (Lovelace, 2015; Wells & Lovelace, 2017), additional experiments with the sUAS to explore ways to adjusting the thermal image opacity in the images capture by thermal camera to decrease the intensity of thermal images could produce a better image. The ability to adjusting the opacity in the overlay image increases the visibility of defects in the thermal image on the screen of the ground control station but the images captured have less resolution. A thermal camera with higher pixel density would provide greater detail as well. The importance of optimizing the thermal and RGB low-light images are crucial in condition where smoke, dust, and fog exist that affect the RGB lowlight camera. Further examination of the ability of the thermal camera to observe defects in structure steel during low visibility conditions should be explored.

3-dementional modeling using photogrammetry software is an increasing focus for UAV-RS. UAVs have the unique ability to rapidly acquire photographs and video from a multitude of perspectives and covert 2-demnsional images using photogrammetry software into a 3-demnsional model. Cho *et al.* (2015) stated is an article on 3D as-is

building modeling for energy modeling purposes, there are three sequential steps to 3D modeling: data collection, modeling, and analysis. These steps are identical for modeling the structure of a bridge as well.

In a recent evaluation of commercially available remote sensors for bridge inspections (Vaghefi *et al.*, 2018) found 3-dimensional photogrammetry was ideal for bridge global metrics of a change in bridge length; vertical movement of a bridge due to settlement; bridge movement in transverse directions, and surface roughness.

Furthermore, 3D photogrammetry and Thermal imaging were sufficient in detecting surface cracks in steel and concrete girders as well as steel and concrete section loss. The global metrics along with the surface cracks and section losses are symptomatic of a bridges condition following a large disaster event and are critical in determining the scope of damage to a bridge.

Khodaei *et al.* (2015) study use of a UAV equipped with a thermal camera to create 3D digital surface model (DSM) from thermal video imagery. The process involved using a scale-invariant feature transformation (SIFT) algorithm to tie points from unordered frames of video to orient the extracted frames. The results found a comparable accuracy with the thermal DSM was a smooth image. Recommends further investigation of thermal in combination with visible images.

Chan *et al.* (2017) found the 3D model of a steel truss bridge significantly improve the amount of information able to multiple parties to contextualize the current condition on the bridge. Furthermore, the study found D models reduced the need to re-inspect and reduced the costs associated with traditional methods of inspection.

Most scientific studies have focused on using UAV-RS to generate 2D images for 3D models during hours of daylight. Further research is needed to present evidence of using low-light and thermal imagery from sUAS during limited visibility conditions to create 3D models for structural analysis of steel bridges.

Nationwide, of the 615,002 bridges in United States, approximately 40 percent are 50 years old or older and an additional 15 percent between 40 and 49 years old (ASCE, 2017). Of the 337,312 bridges 40-years-old and older, 9.1 percent are deemed structurally deficient as of 2016 and carry an estimated 188 million trips per day across them (ASCE, 2017 & Lee *et al.*, 2103). Bridges designed for a specified load 50 years ago are now subject to loads at or over the original design capacity more frequently. Investigating semi-autonomous flight couple with computer vision software would be another valuable area during low-light conditions. Duatre *et al.* (2017) found their proposed framework using convolution neural network using imagery from UAVs increased the efficiency in detecting damage to buildings exterior facades by reducing the number images required. Cha *et al.* (2017) found their framework using convolution neural networks promising in the detecting of crack damage in concrete. Vetrivel *et al.* (2018) framework for training a supervised model based on convolution neural network (CNN) using UAV imagery was significant in detecting damage and a model trained with enough samples was transferable without having to retrain. Training optical system of the sUAS to recognize damage and defects in structure steel would improve upon current studies using sUAS for Structural inspection.

Future research should seek to build on the information provided from this study and incorporate semi-autonomous inspection of bridge critical components with flight

planning software couple with computer vision in low-light conditions to determine the capabilities of semi-autonomous inspection for structural damage in low-light conditions. The sUAS low-light imagery from this study can be used to train computer vision software to determine damage and defects in structural steel, speed for semi-autonomous flight. Furthermore, research involving differing ground and visibility (i.e. smoke, fog, dust...) conditions should be conducted to build the capacity of sUAS using computer vision to determining damage and defects in structure steel.

5.5 Summary

The aim of the research was to answer the three research questions:

1. What is the effect of low-light conditions on the sUAS optics to assess global structural damage?
2. What effect does distance have on the sUAS camera imagery in observing damage and defects in the structural steel during low-light conditions?
3. What is the logical correlation, if any, between the sUAS camera imagery to observe damage and defects during low-light conditions at a given distance?

The imagery collected by the sUAS, data collected based off the imagery, and data analyzed, presented and discussed, have answered the research questions, although further research is needed. The effects of low-light conditions on the sUAS optics ability to detect damage and defects on steel girders were analyzed and differences in capabilities between the RGB low-light and thermal imaging camera were discovered. From answering these three research questions more questions have arisen. Still, important information has been discovered through this research. The knowledge gained in the ability to inspect structural steel in low-light conditions gives practitioners the

ability to investigate structures during hours of darkness for damage and defects. This new knowledge opens new areas to explore in using sUAS to be effectively used for inspection during low-light conditions.

The capability to inspect structures during hours of darkness has the potential to decrease response and recovery time following a disaster by providing better situational awareness of the state of transportation infrastructure. The capability to assess damage and defects around the clock following a disaster event could reduce the number of casualties and speed up recovery operations. Further study of the use of sUAS in low-light conditions for structural damage assessments would be beneficial for disaster recovery for practitioners.

REFERENCES

- ASTM, (2013). Standard specification for structural steel for bridges. West Conshohocken: American Society for Testing and Materials. A709/A709M.
- American Society of Civil Engineers (2017): *Report card for America's infrastructure*. American Society of Civil Engineers. Available at <https://www.infrastructurereportcard.org/cat-item/bridges/> Accessed on June 3, 2018
- Adams, S., Friedland, C., & Levitan, M. (2010). *Unmanned aerial vehicle data acquisition for damage assessment in hurricane events*. Research Gate. 1-8
<https://www.researchgate.net/publication/228453510>. Accessed June 2, 2018
- Adams, S., & Friedland, C. (2011). *A survey of unmanned aerial vehicle (UAV) usage for imagery collection in disaster research and management*. Research Gate. 1-9
<https://www.researchgate.net/publication/266465037> Accessed June 2, 2018
- Baker C., Rapp, R., Elwakil, E., & Zhang, J. (in-press). *Infrastructure assessment post-disaster: remotely sensing bridge structural damage by unmanned aerial vehicle in low-light conditions*. Journal of Emergency Management.
- Barfuss, S. L., Jensen, A. and Clemens, S. (2012). *Evaluation and development of (UAV) for UDOT needs*. Prepared for: Utah Department of Transportation.
- Baroudi, B., & R. Rapp, R. (2014). *Stakeholder management in disaster restoration projects*. International Journal of Disaster Resilience in the Built Environment, 5(2), 182-193. doi:10.1108/IJDRBE-07-2012-0021
- Boyd, D. & Chinyio, E. (2008). *Understanding the construction client*. John Wiley & Sons.
- Brooks C., Dobson, R., Banach, D., Dean, D., Oommen, T., Wolf, R., Havens, T., Ahlborn, T., & Hart, B. (2015). *Evaluating the use of unmanned aerial vehicles for transportation purposes*. Michigan Tech Research Institute, Ann Arbor, MI.
- Carvajal, F., Agüera, F., & Pérez, M., (2011). *Surveying a landslide in a road embankment using unmanned aerial vehicle photogrammetry*. ISPRS – Int. Arch. Photogrammetry Remote Sens. Spatial Inform. Sci. XXXVIII-1/C22, 201–206.
- Cha, Y., Choi, W. & Büyüköztürk, O. (2017). *Deep Learning-Based Crack Damage Detection Using Convolutional Neural Networks*. Computer-Aided Civil and Infrastructure Engineering, 32: 361-378. doi:10.1111/mice.12263
- Chan, B., Saul, I., Pettigrew, T., & Anstice, D. (2017) *Photogrammetric modelling for bridge inspection and remediation*. 8th Australian Small Bridges Conference.

- Chang, Y., Wilkinson, S., Potangaroa, R., & Seville, E. (2012). *Managing resources in disaster recovery projects*. *Engineering, Construction and Architectural Management*, 19(5), 557-580. doi:10.1108/09699981211259621
- Chang, Y., Wilkinson, S., Potangaroa, R., & Seville, E. (2012). *Resourcing for post-disaster reconstruction: A comparative study of Indonesia and china*. *Disaster Prevention and Management*, 21(1), 7-21.
doi:http://dx.doi.org.ezproxy.lib.purdue.edu/10.1108/09653561211202674
- Chang-Richards, Y., Wilkinson, S., Potangaroa, R., & Seville, E. (2013). *Resource challenges for housing reconstruction*. *Disaster Prevention and Management*, 22(2), 172-181.
- Cho, Y.K., Ham, Y., & Golpavar-Fard, M. (2015). *3D as-is building energy modeling and diagnostics: A review of the state-of-the-art*. *Advanced Engineering Informatics*, 29, 184-195.
- Chou, T., Yeh, M., Chen, Y., & Chen, Y. (2010). *Disaster monitoring and management by the unmanned aerial vehicle technology*. ISPRS Technical Commission VII Symposium. (Vienna) 2010. 38(7B)
- Colomina, I., & Molina, P. (2014). *Unmanned aerial systems for photogrammetry and remote sensing: A review*. *ISPRS Journal of Photogrammetry and Remote Sensing*, 92, 79-97. doi:10.1016/j.isprsjprs.2014.02.013
- Comfort, L. K. (2007). *Inter-organizational design for disaster management: Cognition, communication, coordination and control*. *Journal of Seismology and Earthquake Engineering*, 9(1-2), 61-71. Retrieved from <https://search-proquest-com.ezproxy.lib.purdue.edu/docview/1687373042?accountid=133>
- Department of Homeland Security. (2013). *National response framework*. 2nd ed. Washington, D.C.: Department of Homeland Security.
- Department of Homeland Security. (2004). *National response plan*. Washington, D.C.: Department of Homeland Security.
- Dorafshan, S. & Maguire, M. (2017). *Challenges in bridge inspection using small unmanned aerial systems: Results and lessons learned*. Proc. 2017 International Conference on Unmanned Aircraft Systems (ICUAS), Miami, FL. DOI:10.1109/ICUAS.2017.7991459
- Duarte, D., Nex, F., Kerle, N., & Vosselman, G. (2017). *Towards a more efficient detection of earthquake induced facade damages using oblique UAV imagery*. *Int. Arch. Photogramm. Remote Sens. Spatial Inf. Sci.*, XLII-2/W6, 93-100, <https://doi.org/10.5194/isprs-archives-XLII-2-W6-93-2017>.
- Duverneuil, B. (2016). *Unmanned Aerial Vehicles in Response to Natural Disasters*. *Aerial Drone Archaeology and Preservation*.

- Emissivity in the Infrared, (2018). *Emissivity values*. <http://www.optotherm.com/emiss-table.htm>
Accessed June 20, 2018
- Erdelj, M., Natalizio, E., Chowdhury, K., & Akyildiz, I. (2017). *Help from the sky: Leveraging UAVs for disaster management*. Pervasive Computing. IEEE CS: 24 -32
- Escobar-Wolf, R., Oommen, T., Brooks, C.N., Dobson, R.J., & Ahlborn, T.M. (2017). *Unmanned aerial vehicle (UAV)-based assessment of concrete bridge deck delaminations using thermal and visible camera sensors: A preliminary analysis*. Research in Nondestructive Evaluation, Taylor & Francis. doi/abs/10.1080/09349847.2017.1304597
- Farhey, D. (2018). *Structural performances of bridge types in the U.S. national bridge inventory*. MDPI, Basel, Switzerland. This article is an open access article distributed under the terms and conditions of the Creative Commons Attribution (CC BY) license (<http://creativecommons.org/licenses/by/4.0/>).
- Farhey, D. (2018). *Material structural deficiencies of road bridges in the U.S. Infrastructures*. MDPI, Basel, Switzerland. This article is an open access article distributed under the terms and conditions of the Creative Commons Attribution (CC BY) license (<http://creativecommons.org/licenses/by/4.0/>).
- Gillins, D. T., Parrish, C., Gillins, M. N., & Simpson, C. (2018). *Eyes in the Sky: Bridge Inspections with Unmanned Aerial Vehicles*. (Report Number: FHWA-OR-RD-18-11) Oregon Department of Transportation Research Section & Federal Highway Administration.
- Hongxia, L., & Qi, F. (2016). *Application of UAV in the field management of construction project*. RISTI - Revista Iberica De Sistemas e Tecnologias De Informacao, 2016 (18), 235-243. doi:10.17013/risti.18A.235-243
- Hu, J. P., Wu, W. B., & Tan, Q. L. (2012). *Application of unmanned aerial vehicle remote sensing for geological disaster reconnaissance along transportation lines: A case study*. Applied Mechanics and Materials Vols. 226-228, 2376-2379
doi:10.4028/www.scientific.net/AMM.226-228.2376
- Irizarry, J., & Johnson, E.N. (2014) *Feasibility study to determine the economic and operational benefits of utilizing aerial vehicles (UAVs)* (Georgia DOT Research Project Report No. FHWA-GA-1H-12-38). pp 158. Georgia Department of Transportation, Atlanta, GA
- Jansen, G. (2015). *Drone companies set sights on construction industry*. Concrete International, 34-35. Retrieved from <https://search-proquest-coSaffarzadeh>
- A., Shimaoka, T., Nakayama, H., Hanashima, T., Yamaguchi, K., & Manabe, K. (2017). *Tasks and problems involved in the handling of disaster waste upon April 2016 Kumamoto earthquake, Japan*. Natural Hazards, 1-18. doi:10.1007/s11069-017-3021-1

- Karunasena, G., & Amaratunga, D. (2016). *Capacity building for post disaster construction and demolition waste management*. *Disaster Prevention and Management*, 25(2), 137-153. Retrieved from doi:<http://dx.doi.org.ezproxy.lib.purdue.edu/10.1108/09653561311325316>
- Katel, P. (2006, February 3). *Rebuilding New Orleans*. *CQ Researcher*, 16, 97-120. Retrieved from <http://library.cqpress.com.ezproxy.lib.purdue.edu/>
- Kim, J. O., & Lee, J. K. (2017). *UAV application for process control of the reclamation project*. *Journal of Coastal Research*, 33(Special Issue 79), 309-313. doi:10.2112/SI79-063.1
- Knabb, R. D., Rhome, J. R., & Brown, D. P. (2005) *Tropical cyclone report: Hurricane Katrina*. National Hurricane Center. 20 December 2005. Retrieved from <https://search.usa.gov/search?utf8=%E2%9C%93&affiliate=noaa.gov&query=hurricane+katrina+stats>
- Lee, G., Mohan, S., Huang, C., & Fard, B. (2013). *A study of U.S. bridge failures (1980-2012)*". Technical Report MCEER-13-0008. (Buffalo).
- Lovelace, B. (2015) *Unmanned aerial vehicle bridge inspection demonstration project* (Minnesota DOT Report No. MN/RC 2015-40). Minnesota Department of Transportation
- Lloyd-Jones, Tony. (2006). *Mind the Gap! Post-disaster reconstruction and the transition from humanitarian relief*. Summary report for RICS by the Max Lock Centre at the University of Westminster.
- Luther, L. (2006). *Disaster debris removal after Hurricane Katrina: Status and associated issues*. Washington, D.C.: Congressional Research Service.
- McCormack, E.D. (2008) *The use of small unmanned aircraft by the Washington State Department of Transportation* (Research Report). Washington State Transportation Center (TRAC), Seattle, WA.
- McEntire, D. A., Webb, G., & Burdick, B. (2015). *Planning and improvisation in emergency management*. In Trainor, J. E. & Subbio, T. (Eds.), *Critical Issues in Disaster Science and Management: A Dialogue Between Researchers and Practitioners* (pp. 193 – 222). Washington, D.C.: FEMA
- McGuire, M., Rys, M.J. & Rys, A. (2016) *A study of how unmanned aircraft systems can support the Kansas Department of Transportation's efforts to improve efficiency, safety, and cost reduction* (PublicationNo. K-TRAN: KSU-15-3). Kansas Department of Transportation.
- Melo, R. d., Costa, D. B., Álvares, J. S., & Irizarry, J. (2017). *Applicability of unmanned aerial system (UAS) for safety inspection on construction sites*. *Safety Science*, 98174-185. doi:10.1016/j.ssci.2017.06.008

- Murphy, R. R., Steimle, E., Griffin, C., Cullins, C., Hall, M. and Pratt, K. (2008), *Cooperative use of unmanned sea surface and micro aerial vehicles at Hurricane Wilma*. Journal of Field Robotics, 25: 164–180. doi: 10.1002/rob.20235
- National Oceanic and Atmospheric Administration, U.S. Department of Commerce (2017) <https://oceanservice.noaa.gov/facts/remotesensing.html>
- NOAA National Centers for Environmental Information (NCEI), (2018). *U.S. billion-dollar weather and climate disasters*. <https://www.ncdc.noaa.gov/billions/> (accessed on July 20, 2018)
- Omar, T., & Nehdi, M. L. (2017). *Remote sensing of concrete bridge decks using unmanned aerial vehicle infrared thermography*. Automation in Construction, 83, 360-371. doi:10.1016/j.autcon.2017.06.024
- Otero, L.D., Gagliardo, N., Dalli, D., Huang, W. H. & Cosentino, P. (2015) *Proof of concept for using unmanned aerial vehicles for high mast pole and bridge inspections* (Publication No. BDV28 TWO 977-02). Florida Institute of Technology.
- Pratt, K., R. R. Murphy, et al. (2006). *Overview of the requirements for Semi-Autonomous Flight in Miniature UAVs for Structural Inspection*. AUVSI's Unmanned Systems North America. Orlando, Florida, Association for Unmanned Vehicle Systems International. http://www.kpratt.net/wp-content/uploads/2006/09/KPratt_AUVSI_2006_Semi-Autonomy.pdf Accessed on June 1, 2018
- Rapp, R., R., (2008). *Complex Urgency: Recovering from Katrina and Wilma*. AACE International Transactions ADV.02, AD21.
- Rau, J., Jhan, J., Lob, C., Linb, Y., 2011. *Landslide mapping using imagery acquired by a fixed-wing UAV*. ISPRS – Int. Arch. Photogramm. Remote Sens. Spatial Inform. Sci. XXXVIII-1/C22, 195–200
- Ryan, T., Mann, E., Chill, Z., Ott, B. (2012). *Bridge inspector's manual (BIRM)*. Federal Highway Administration, National Highway Institute (Arlington).
- Siebert, S., Teizer J., (2014). *Mobile 3-D mapping for surveying earthwork project using an unmanned aerial vehicle (uav) system*. Automation in Construction, 41, 1-14. doi:10.1016/j.autcon.2014.01.004
- Smith, A., & Katz, R. (2013). *U.S. billion-dollar weather and climate disasters: Data sources, trends, accuracy and biases*. Natural Hazards: 67(2) 387-410 DOI: 10.1007/s11069-013-0566-5
- Smith, G. (2010). *Lessons from the United States: Planning for post-disaster recovery and reconstruction*. The Australasian Journal of Disaster and Trauma Studies, 2010 - 1

- Tanzi, T. J., Chandra, M., Isnard, J., Camara, D., Olivier, S., & Harivelo, F. (2016). *Towards "drone-borne" disaster management: Future application scenarios*. ISPRS Annals of the Photogrammetry, Remote Sensing and Spatial Information Sciences, Iii-8, 181-189. doi:<http://dx.doi.org.ezproxy.lib.purdue.edu/10.5194/isprs-annals-Iii-8-181-2016>
- TRN, 2005. *Review of tsunami recovery*. London: Tsunami Recovery Network (TRN) and Development Planning Unit, University College London.
- United States Naval Observatory, (2018) *Rise, set, and twilight definitions*. Naval Oceanography Portal. 2018 http://aa.usno.navy.mil/faq/docs/RST_defs.php Accessed June 2, 2018
- U. S. Department of Transportation, (2010). *Bureau of transportation statistics: Freight facts and figures*. <http://www.fhwa.dot.gov/pressroom/fhwa1062.htm> Accessed on June 4, 2018
- Vaghefi, K., Oats, R., C., Harris, D., K., Ahlborn, T., M., Brooks, C., N., Endsley, K, A., Roussi, C., Shuchman, R., Burns, J., W., & Dobson, R. (2012). *Evaluation of commercially available remote sensors for highway bridge condition assessment*. Journal of Bridge Engineering. 17(6): 886-895.
- Vetrivel, A., Gerke, M., Kerle, N., Nex, F., & Vosselman, G. (2018). *Disaster damage detection through synergistic use of deep learning and 3D point cloud features derived from very high resolution oblique aerial images, and multiple-kernel-learning*. ISPRS Journal of Photogrammetry and Remote Sensing, Volume 140, 45-59, ISSN 0924-2716, <https://doi.org/10.1016/j.isprsjprs.2017.03.001>.
- Wells, J., & Lovelace, B. (2017) *Unmanned aircraft system bridge inspection demonstration project phase II* (Research Project Final Report 2017-18, 2017). Minnesota Department of Transportation.
- Yamamoto, T, Kusumoto, H, & Banjo, K. (2014) *Data Collection System for a rapid recovery work: Using digital photogrammetry and a small unmanned aerial vehicle (UAV)*. Computing in Civil and Building Engineering, Reston, VA. 875-882
- Zhang, Y., & Peacock, W. G. (2010). *Planning for housing recovery?* American Planning Association. Journal of the American Planning Association, 76(1), 5-24. Retrieved from <https://search-proques.com.ezproxy.lib.purdue.edu/docview/229653005?accountid=13>

PUBLICATION

Baker C., Rapp, R., Elwakil, E., & Zhang, J. (in-press). *Infrastructure assessment post-disaster: remotely sensing bridge structural damage by unmanned aerial vehicle in low-light conditions*. Journal of Emergency Management.